

# Running effects on neutrino parameters and $\ell_i \rightarrow \ell_j \gamma$ predictions in the triplet-extended MSSM

F.R. Joaquim<sup>1</sup>

*CERN, Theory Division,  
CH-1211 Geneva 23, Switzerland*

*E-mail:* [Filipe.Joaquim@cern.ch](mailto:Filipe.Joaquim@cern.ch)

**ABSTRACT:** We investigate the renormalisation group effects induced on neutrino mass and mixing parameters in a triplet-extended minimal supersymmetric standard model where a vector-like pair of hypercharge  $\pm 1$  triplet superfields is added. We first rederive the one-loop renormalisation group equation for the effective neutrino mass operator and, for the case in which this operator originates solely from the decoupling of the triplets, the corresponding equations for neutrino masses, mixing parameters and CP-violating phases. We compare our results with the ones obtained previously, and quantify the importance of the RG induced corrections to neutrino observables by means of numerical examples. In the second part of the paper, we study the correlation of the model's predictions for the lepton flavour violating processes  $\ell_i \rightarrow \ell_j \gamma$  with the measured neutrino mass squared differences and mixing angles. We also emphasize the rôle played by the unknown reactor neutrino mixing angle  $\theta_{13}$  and the Dirac CP-violating phase  $\delta$ . We point out that, if  $\tan \beta$  is large, the results obtained in the commonly made approximations may deviate significantly from the ones following from solving numerically the relevant set of renormalisation group equations and using the exact one-loop formulae for the decay rates.

**KEYWORDS:** Rare Decays, Neutrino Physics, Supersymmetric Standard Model, Renormalization Group

---

<sup>1</sup>On leave from the “Centro de Física Teórica de Partículas (CFTP)”, Lisbon, Portugal.

---

**Contents**

<b>1</b>	<b>Introduction</b>	<b>1</b>
<b>2</b>	<b>RGE for the effective neutrino mass operator</b>	<b>3</b>
<b>3</b>	<b>Running of the neutrino masses and mixing matrix</b>	<b>6</b>
<b>4</b>	<b>The pure type II seesaw case</b>	<b>7</b>
4.1	RGEs for the neutrino masses, mixing angles and CP-violating phases	9
4.2	Numerical examples	14
<b>5</b>	<b>LFV <math>\ell_i \rightarrow \ell_j \gamma</math> decays in the TMSSM</b>	<b>17</b>
5.1	Approximate predictions for the $\ell_i \rightarrow \ell_j \gamma$ rates	17
5.2	Large $\tan \beta$ effects on the ratios of branching ratios	22
<b>6</b>	<b>Summary and concluding remarks</b>	<b>27</b>

---

**1 Introduction**

One of the most puzzling and longstanding problems in particle physics concerns the explanation of the observed fermion mass and mixing patterns. The interest around this subject has been renewed with the confirmation that neutrinos are massive. This motivated intense activity towards the search for an answer to the question on how neutrinos acquire their tiny mass. From the theoretical point of view, the idea that neutrino masses are suppressed by a large energy scale has become the most popular one. This is the basis of the well-known seesaw mechanism [1–5] for neutrino mass generation. The phenomenology of seesaw-inspired models has been widely studied in the literature [6–8] with the goal of explaining the results provided by neutrino oscillation experiments [9, 10].

If the mechanism generating neutrino masses operates at high-energy scales, renormalisation group (RG) effects may induce important corrections to the neutrino parameters. Several analyses devoted to the study of the neutrino parameter running have supported this expectation [11]. The RG corrections to the effective neutrino mass operator depend crucially on the properties of the neutrino mass spectrum, on the absolute neutrino mass scale and on the size of the  $\tau$  Yukawa coupling. Therefore, the running of the neutrino parameters is expected to be enhanced in supersymmetric (SUSY) models with large  $\tan \beta$ . For instance, neutrino mixing may be strongly augmented by the running from high to low energies [12, 13] so that bimaximal neutrino mixing at high scales can be made compatible with low-energy neutrino data by including RG corrections [14, 15]. Ultimately, with the gradual increasing of neutrino data precision, even small RG effects may turn out to be important for neutrino mass and mixing model building.

Within seesaw-based scenarios, the RG flow above the decoupling scale of the heavy *seesaw mediators* has to be properly accounted for, including possible threshold effects due to the presence of different mass scales. This has been done in refs. [16–18] in the framework of the so-called type I seesaw mechanism [1–5] where the heavy degrees of freedom responsible for the suppression of neutrino masses are singlets under the Standard Model (SM) gauge group. The results of such studies are model dependent since the RG effects above and between the thresholds depend on the Yukawa couplings of the heavy neutrino singlets with the leptons and Higgs fields, which cannot be reconstructed from low-energy data. Hence, the impact of the RG corrections strongly depends on the structure of the unknown fundamental couplings which is encoded in the effective neutrino mass operator. The impossibility of reconstructing in a model-independent way the high-scale neutrino sector parameters from low-energy measurements of masses and mixing angles is the main problem of the type I seesaw mechanism.

An alternative version of the seesaw mechanism (usually denoted as type II or triplet seesaw) relies on the presence of heavy triplet states [19–25]. Its SM version requires a single scalar triplet to generate mass for the three light neutrinos. In the minimal supersymmetric standard model (MSSM) a vector-like pair of hypercharge  $\pm 1$  triplet superfields is demanded to ensure anomaly cancelation and holomorphicity of the superpotential. The analysis of the RG effects on neutrino parameters in the SM type II seesaw has been presented in ref. [26]. A more complete study covering both the SM and SUSY cases can be found in ref. [27]. However, the RGEs for the triplet-extended MSSM (TMSSM) derived in that paper differ from the ones obtained in refs. [28] and [29].

The couplings of the *seesaw mediators* to the SM lepton doublets and/or Higgses may induce lepton flavour violation (LFV) in the soft SUSY-breaking Lagrangian, even if the mechanism which breaks SUSY is flavour blind [28, 30]. If large enough, such LFV effects can drastically increase the rates of LFV processes (like radiative charged-lepton decays  $\ell_i \rightarrow \ell_j \gamma$ ), which are otherwise suppressed to levels well beyond the sensitivity of future experiments. Complementarity studies between low-energy neutrino physics and LFV decay searches have been carried out in the context of the SUSY type I [31] and type II [28, 32–36] seesaw mechanisms. The main difference between these two approaches is that the triplet seesaw is much more predictive when it comes to establishing a connection between low-energy neutrino physics and LFV decay searches.

In this work we will investigate several aspects of the RG running of neutrino parameters (masses, mixing angles and CP-violating phases) in the TMSSM, where neutrino masses are suppressed via the type II seesaw mechanism. The impact of the RG effects on predictions for the branching ratios of the LFV decays  $\ell_i \rightarrow \ell_j \gamma$  will be also discussed and illustrated with several examples. The layout of the paper is as follows: in section 2 we derive the RGE for the dimension-five effective neutrino mass operator in the framework of an SU(5) grand-unified model in which the heavy-triplet superfields are naturally embedded. The general form of the RGEs for the neutrino masses and mixing matrix is obtained in section 3. Section 4 is devoted to the study of the neutrino parameter running in the pure type II seesaw case. Namely, in section 4.1 we obtain the RGEs for the neutrino masses, mixing angles and CP-violating phases (including approximate analytical expres-

sions), pointing out the discrepancies between our results and those previously obtained in ref. [27]. Some numerical examples are presented in section 4.2. In the second part of the paper we discuss predictions of the considered model for the LFV radiative decays  $\ell_i \rightarrow \ell_j \gamma$  taking into account the latest neutrino oscillation data. We begin in section 5.1 by presenting the rates of these decays obtained with the help of the frequently made approximation which neglects the RG running of the neutrino sector parameters, treats in a simplified way the running of the slepton mass matrices and uses a simplified formula for the  $\ell_i \rightarrow \ell_j \gamma$  decay rates. In section 5.2 these results are compared with the ones of an improved approximation in which the running of the neutrino parameters is taken into account and with the results obtained by solving numerically the full set of RGEs and by computing the decay amplitudes using the exact one-loop formulae. This allows us to quantify how much the approximate results of section 5.1 deviate from the more accurate approaches. In particular, we show that in some cases the splitting of slepton masses generated by the RG running can also be important.

## 2 RGE for the effective neutrino mass operator

Let us consider a supersymmetric N=1 Yang-Mills model with a superpotential of the form:

$$W = \frac{Y^{ijk}}{3!} \Phi_i \Phi_j \Phi_k + \frac{\mu^{ij}}{2} \Phi_i \Phi_j + \frac{\mathcal{O}^{abcd}}{4!} \Phi_a \Phi_b \Phi_c \Phi_d, \quad (2.1)$$

where the chiral superfields  $\Phi_i$  contain a complex scalar  $\phi_i$  and a two-component fermion  $\psi_i$ , which transform as a representation  $R_i = R_i^1 \otimes \dots \otimes R_i^n$  of the gauge group  $G = G_1 \times \dots \times G_n$ . The first two terms in the above superpotential are the ordinary Yukawa and mass terms and  $\mathcal{O}$  is a non-renormalisable operator suppressed by the inverse of a large mass scale. Provided that higher-dimensional non-renormalisable operators only appear in the superpotential, then the SUSY non-renormalisation theorem still holds [37]. Consequently, the operator  $\mathcal{O}$  can be renormalised taking into account only wave-function renormalisation. Using the one-loop anomalous-dimension matrices for the chiral superfields [38]

$$\gamma_i^{(1)j} = \frac{1}{32\pi^2} \left[ Y_{ipq} Y^{j pq} - 4\delta_i^j \sum_k g_k^2 C_k(i) \right], \quad Y_{ipq} \equiv (Y^{ipq})^*, \quad (2.2)$$

and following for instance refs. [39, 40], one can write the one-loop RGE for the operator  $\mathcal{O}$  as:<sup>1</sup>

$$\dot{\mathcal{O}}^{abcd} = \mathcal{O}^{abcf} \gamma_f^{(1)d} + (a \leftrightarrow d) + (b \leftrightarrow d) + (c \leftrightarrow d). \quad (2.3)$$

The quantities  $g_k$  are the gauge coupling constants of the sub-groups  $G_k$  of  $G$  and  $C_k(i)$  denotes the corresponding quadratic Casimir invariant of the irreducible representation of  $\Phi_i$ .

We now consider an extension of the MSSM where a vector-like pair of triplet supermultiplets  $T$  and  $\bar{T}$  transforming under the  $SU(3)_c \times SU(2) \times U(1)_Y$  SM gauge group as  $T \sim (1, 3, 1)$  and  $\bar{T} \sim (1, 3, -1)$  is added. In a grand-unified theory (GUT) these triplet

---

<sup>1</sup>From now on we will denote by  $\dot{X}$  the derivative of the quantity  $X$  with respect to  $t = \ln(\Lambda/\Lambda_0)$ , where  $\Lambda$  is the renormalisation scale and  $\Lambda_0$  is a fixed but arbitrary reference mass scale.

states may be part of the gauge group representation. For instance, in the SU(5) GUT,  $T$  and  $\bar{T}$  are part of the  $\mathbf{15}$  and  $\overline{\mathbf{15}}$  representations, respectively. In this case, one has  $\mathbf{15} = T \oplus S \oplus Z$  where  $S \sim (6, 1, -2/3)$  and  $Z \sim (3, 2, 1/6)$  under the SM gauge group.

Below the GUT scale, the superpotential reads:

$$\begin{aligned}
 W &= W_0 + W_T + W_{S,Z}, \\
 W_0 &= Y_e e^c H_1 L + Y_d d^c H_1 Q + Y_u u^c Q H_2 + \mu H_2 H_1, \\
 W_T &= \frac{1}{\sqrt{2}}(Y_T L T L + \lambda_1 H_1 T H_1 + \lambda_2 H_2 \bar{T} H_2) + M_T \text{Tr}[(i\sigma_2)T(i\sigma_2)\bar{T}], \\
 W_{S,Z} &= \frac{1}{\sqrt{2}}Y_S d^c S d^c + Y_Z d^c Z L + M_Z Z \bar{Z} + M_S S \bar{S},
 \end{aligned} \tag{2.4}$$

where  $L$  ( $Q$ ) is the lepton (quark) doublet supermultiplet and  $e^c$ ,  $d^c$  and  $u^c$  are the charged-lepton and quark singlet supermultiplets. The MSSM superpotential is denoted by  $W_0$  while  $W_T$  ( $W_{S,Z}$ ) contains the couplings of  $T, \bar{T}$  ( $S, Z$ ) with the MSSM superfields, including the corresponding mass terms. We adopt the SU(2) representation for the triplet superfields<sup>2</sup>

$$T = (i\sigma_2) \frac{\sigma_i T_i}{\sqrt{2}} = \begin{pmatrix} T^0 & -\frac{T^+}{\sqrt{2}} \\ -\frac{T^+}{\sqrt{2}} & -T^{++} \end{pmatrix}, \quad \bar{T} = (i\sigma_2) \frac{\sigma_i \bar{T}_i}{\sqrt{2}} = \begin{pmatrix} \bar{T}^{--} & -\frac{\bar{T}^-}{\sqrt{2}} \\ -\frac{\bar{T}^-}{\sqrt{2}} & -\bar{T}^0 \end{pmatrix}. \tag{2.5}$$

To keep the discussion as general as possible, we will consider that an effective neutrino mass operator of the form [41]:

$$W_\nu = \frac{1}{2} \mathcal{O}_{ij}^\nu \epsilon_{ab} \epsilon_{cd} L_i^a H_2^b L_j^c H_2^d, \tag{2.6}$$

is also present in the superpotential. In the above equation,  $i, j$  and  $a, b, c, d$  are family and SU(2) indices, respectively. Notice that we neglect possible effective dimension-four Kähler operators of the type  $(L_i \cdot H_2)(L_j \cdot \bar{H}_1)/M^2$  or  $(L_i \cdot \bar{H}_1)(L_j \cdot H_2)/M^2$  (where  $M$  is some very large scale) which could also give rise to an effective neutrino mass term after electroweak symmetry breaking (EWSB). The phenomenology of Kähler-generated neutrino masses (including the RG flow of neutrino parameters) has been studied in refs. [42, 43]. Here we assume that these contributions are irrelevant because they are suppressed by extra  $1/M$  factors compared with the contributions of the operators included in  $W_\nu$ .

The RGEs for all coupling and mass parameters in (2.4) can be found in refs. [28] and [29]. We have recomputed the full set of RGEs and found complete agreement with the results obtained in the latter reference.<sup>3</sup> Using eq. (2.3) we obtain the one-loop RGE for  $\mathcal{O}^\nu$  in (2.6) as

$$\dot{\mathcal{O}}_{ij}^\nu = 2\gamma_{H_2}^{(1)H_2} \mathcal{O}_{ij}^\nu + \mathcal{O}_{ik}^\nu \gamma_{L_k}^{(1)L_j} + \gamma_{L_k}^{(1)L_i} \mathcal{O}_{kj}^\nu. \tag{2.7}$$

<sup>2</sup>The representations of  $S$  and  $Z$  can be found in ref. [28].

<sup>3</sup>The RGEs obtained in ref. [29] show minor differences with respect to those of [28]. See [29] for more details.

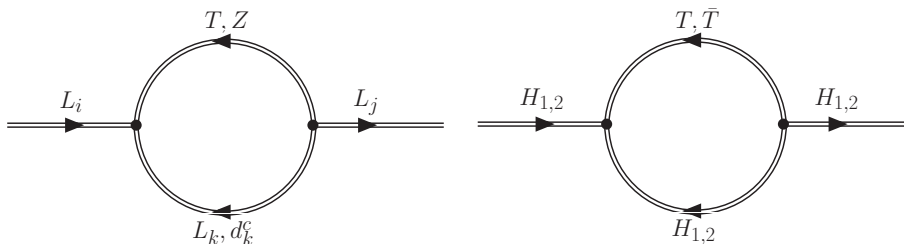


**Figure 1.** One-loop (non MSSM) supergraphs relevant for wave-function renormalisation of the lepton (left diagram) and Higgs (right diagram) doublet superfields under the superpotential (2.4).

The one-loop anomalous dimensions for  $L$  and  $H_{1,2}$  can be computed from eqs. (2.2) and (2.4), yielding the result:

$$16\pi^2 \gamma_{L_i}^{(1)L_j} = \left[ Y_e^\dagger Y_e + \underline{3Y_T^\dagger Y_T} + \underline{3Y_Z^\dagger Y_Z} \right]_{ij} - \left( \frac{3}{10}g_1^2 + \frac{3}{2}g_2^2 \right) \delta_i^j, \quad (2.8)$$

$$16\pi^2 \gamma_{H_1}^{(1)H_1} = \text{Tr}(Y_e^\dagger Y_e + 3Y_d^\dagger Y_d) + \underline{3|\lambda_1|^2} - \frac{3}{10}g_1^2 - \frac{3}{2}g_2^2, \quad (2.9)$$

$$16\pi^2 \gamma_{H_2}^{(1)H_2} = 3\text{Tr}(Y_u^\dagger Y_u) + \underline{3|\lambda_2|^2} - \frac{3}{10}g_1^2 - \frac{3}{2}g_2^2, \quad (2.10)$$

where the underlined terms are those absent from the MSSM. These new contributions to the wave-function renormalisation of  $L$  and  $H_{1,2}$  originate from the one-loop supergraphs shown in figure 1. It is straightforward to check that setting  $Y_{T,S,Z} = 0$  and  $\lambda_{1,2} = 0$  in eq. (2.7) one recovers the MSSM RGE for  $\mathcal{O}^\nu$  obtained in refs. [44–46].

After EWSB, the effective neutrino mass matrix

$$m_\nu = \mathcal{O}^\nu v^2 \sin^2 \beta, \quad (2.11)$$

is generated, where  $v = 174 \text{ GeV}$  and  $\tan \beta = \langle H_2^0 \rangle / \langle H_1^0 \rangle = v_2 / v_1$ . Its RGE can be derived from eqs. (2.7)–(2.11), leading to:

$$16\pi^2 \dot{m}_\nu = \alpha_\nu m_\nu + P_\nu^T m_\nu + m_\nu P_\nu, \quad (2.12)$$

where

$$\alpha_\nu = 6\text{Tr}(Y_u^\dagger Y_u) + \underline{6|\lambda_2|^2} - \frac{6}{5}g_1^2 - 6g_2^2, \quad (2.13)$$

$$P_\nu = Y_e^\dagger Y_e + \underline{3Y_T^\dagger Y_T} + \underline{3Y_Z^\dagger Y_Z}. \quad (2.14)$$

When  $T$ ,  $S$  and  $Z$  have different masses, the decoupling of these states has to be performed. In practice, this corresponds to switching off their interactions in the RGEs. At  $\Lambda = M_T$  a new contribution must be added to  $\mathcal{O}^\nu$  due to the decoupling of the triplet fields, in such a way that

$$\mathcal{O}^\nu(M_T) \rightarrow \mathcal{O}^\nu(M_T) + \frac{\lambda_2 Y_T}{M_T} \Big|_{\Lambda=M_T}, \quad (2.15)$$

all quantities being taken at  $\Lambda = M_T$ . Below this scale, the running of the effective neutrino mass matrix follows the RGE (2.12) with  $Y_T = 0$  and  $\lambda_1 = \lambda_2 = 0$ . If  $S$  and/or  $Z$  is lighter

than  $T$ , then it should be subsequently decoupled without adding any contribution to  $\mathcal{O}^\nu$  since this operator arises solely from integrating out the  $SU(2)$  triplets.<sup>4</sup>

### 3 Running of the neutrino masses and mixing matrix

In this section we derive the RGEs for the neutrino masses, the neutrino mixing matrix and the charged-lepton Yukawa couplings in the framework of the model presented in the previous section. We consider that at each scale  $\Lambda$  the following relations hold

$$\begin{aligned} U_\nu^T m_\nu U_\nu &= \text{diag}(m_1, m_2, m_3), & U_e^\dagger Y_e^\dagger Y_e U_e &= \text{diag}(y_e^2, y_\mu^2, y_\tau^2) \equiv d_e^2, \\ U_T^\dagger Y_T^\dagger Y_T U_T &= \text{diag}(y_1^2, y_2^2, y_3^2) \equiv d_T^2, \end{aligned} \quad (3.1)$$

where  $U_e$  and  $U_\nu$  are  $3 \times 3$  complex unitary matrices and  $m_i$  denotes the effective neutrino masses. The neutrino mixing matrix  $U$  at  $\Lambda$  is then given by:

$$U = U_e^\dagger U_\nu. \quad (3.2)$$

To obtain the RGE for  $U$ , we adopt the procedure first introduced in ref. [47] for the renormalisation of the Cabbibo-Kobayashi-Maskawa mixing matrix, and later used for the neutrino case [48–50]. We start by considering the ansatz

$$\dot{U}_e = U_e Q, \quad \dot{U}_\nu = U_\nu R, \quad (3.3)$$

where  $Q$  and  $R$  are anti-Hermitian matrices due to unitarity of  $U_e$  and  $U_\nu$ . In order to determine  $Q$ , one needs the RGE for the charged-lepton Yukawa matrix  $Y_e$ :

$$16\pi^2 \dot{Y}_e = \alpha_e Y_e + Y_e P_e. \quad (3.4)$$

The expressions for  $\alpha_e$  and  $P_e$  are obtained by considering the one-loop anomalous dimensions  $\gamma_{L_i}^{(1)L_j}$  and  $\gamma_{H_1}^{(1)H_1}$  given in eqs. (2.8) and (2.9), respectively, and the same for the charged-lepton singlets  $\gamma_{e_i^c}^{(1)e_j^c} = 2(Y_e^* Y_e^T)_{ij} - 6g_1^2/5\delta_i^j$ . This yields

$$\alpha_e = \text{Tr}(Y_e^\dagger Y_e + 3Y_d^\dagger Y_d) + \underline{3|\lambda_1|^2} - \frac{9}{5}g_1^2 - 3g_2^2, \quad P_e = 3Y_e^\dagger Y_e + \underline{3Y_T^\dagger Y_T} + \underline{3Y_Z^\dagger Y_Z}, \quad (3.5)$$

which, together with the diagonalisation of  $Y_e^\dagger Y_e$  given in (3.1), leads to the following result for  $Q$

$$16\pi^2 Q_{ij} = (P_e')_{ij} \frac{y_{e_i}^2 + y_{e_j}^2}{y_{e_j}^2 - y_{e_i}^2} \quad (i \neq j). \quad (3.6)$$

In this equation,  $P_e'$  is given by

$$P_e' \equiv U_e^\dagger P_e U_e = 3(d_e^2 + U_e^\dagger U_T d_T^2 U_T^\dagger U_e + U_e^\dagger Y_Z^\dagger Y_Z U_e). \quad (3.7)$$

---

<sup>4</sup>In this work we neglect the one-loop threshold corrections to the effective neutrino mass operator arising from the decoupling of the heavy triplet states.

Since  $P'_e$  is Hermitian and  $\alpha_e$  is real, one has  $Q_{ii} = 0$ . Following the same procedure as for  $Q$ , but using now eqs. (2.12)–(2.14) and (3.1), one can derive the expression for the matrix  $R$ :

$$16\pi^2 R_{ij} = \frac{m_i^2 + m_j^2}{m_j^2 - m_i^2} (P'_\nu)_{ij} + \frac{2m_i m_j}{m_j^2 - m_i^2} (P'_\nu)_{ij}^* \quad (i \neq j), \quad (3.8)$$

where  $P'_\nu$  is now defined as:

$$P'_\nu \equiv U_\nu^\dagger P_\nu U_\nu = U^\dagger d_e^2 U + 3(U_\nu^\dagger U_T d_T^2 U_\nu U_T^\dagger + U_\nu^\dagger Y_Z^\dagger Y_Z U_\nu). \quad (3.9)$$

Similarly as for  $Q$ ,  $R_{ii} = 0$  since  $P'_\nu$  is Hermitian and  $\alpha_\nu$  is real. Finally, from eqs. (3.2) and (3.3) (and taking into account that  $Q$  is anti-Hermitian) one obtains:

$$\dot{U} = -QU + UR, \quad (3.10)$$

with  $Q$  and  $R$  given as in eqs. (3.6) and (3.8). The first and second terms on the right-hand side of the above equation account for the contribution to the running of  $U$  coming from  $\dot{U}_e$  and  $\dot{U}_\nu$ , respectively.

As for the neutrino masses  $m_i$ , their RGEs can be derived using eqs. (2.12) and (3.1), leading to:

$$16\pi^2 \dot{m}_i = [\alpha_\nu + 2(P'_\nu)_{ii}] m_i. \quad (3.11)$$

For the charged-lepton Yukawa couplings  $y_{e_i}$  ( $e_i = e, \mu, \tau$ ) the RGE reads

$$16\pi^2 \dot{y}_{e_i} = [\alpha_e + 2(P'_e)_{ii}] y_{e_i}. \quad (3.12)$$

Notice that the presence of the new couplings  $\lambda_1$  and  $Y_{T,Z}$  in  $\alpha_e$  and  $P'_e$  may affect the running of  $y_{e,\mu,\tau}$ .

#### 4 The pure type II seesaw case

In general, the flavour structure and magnitude of the couplings  $Y_{S,Z}$  depend on the specific details of the SU(5) model considered. Although not directly related with  $m_\nu$  at tree-level, these couplings affect the renormalisation of  $Y_T$ . It is worth mentioning that, even if one imposes  $Y_{S,Z} = Y_T$  at *e.g.*  $\Lambda = M_G$  (where from now on  $M_G$  denotes the grand-unification scale), the RG running will deviate  $Y_{S,Z}$  from the  $Y_T$  trajectory. For simplicity, we will restrict ourselves to the case in which the couplings  $Y_{S,Z}$  are negligible when compared with  $Y_T$ . This could for instance result from SU(5) breaking effects, as discussed in ref. [28]. Therefore, from here onwards we set  $Y_{S,Z} = 0$ . Moreover, in the rest of this work we assume that the only contribution to the effective neutrino mass operator  $\mathcal{O}^\nu$  arises from the decoupling of the heavy triplet states  $T$  and  $\bar{T}$ . In other words, we do not address alternative scenarios where extra contributions to the effective neutrino operator are present. Therefore, we have:

$$\mathcal{O}^\nu(M_T) = \frac{\lambda_2 Y_T}{M_T} \Big|_{\Lambda=M_T}, \quad (4.1)$$

at  $\Lambda = M_T$ .



Although  $\mathcal{O}^\nu = 0$  for  $\Lambda > M_T$ , one can define a *would-be* effective neutrino mass operator  $\mathcal{O}^\nu = \lambda_2 Y_T / M$  at any scale  $\Lambda$ . As a consequence of the SUSY non-renormalisation theorem, the RGE of this object coincides with the one given in (2.3). The running of the effective neutrino mass and charged-lepton Yukawa matrices follows the same RGEs as in (2.12) and (3.4), respectively, with:

$$P_\nu = Y_e^\dagger Y_e + 3 Y_T^\dagger Y_T, \quad P_e = 3 Y_e^\dagger Y_e + 3 Y_T^\dagger Y_T. \quad (4.2)$$

Since  $m_\nu$  is now proportional to  $Y_T$ , the unitary matrices  $U_\nu$  and  $U_T$  in eqs. (3.1) are identical and

$$Y_T^\dagger Y_T = \frac{m_\nu^\dagger m_\nu}{v_T^2}, \quad y_i^2 = \frac{m_i^2}{v_T^2}, \quad v_T = \frac{\lambda_2 v_2^2}{M_T}. \quad (4.3)$$

The quantity  $v_T$  is the induced vacuum expectation value of the neutral-scalar component of  $T$ :  $\langle T^0 \rangle = v_T / \sqrt{2}$ . The RGE for the neutrino mixing matrix  $U$  is shown in eq. (3.10) with  $Q$  and  $R$  defined as in eqs. (3.6) and (3.8). Taking into account eqs. (3.1), together with the fact that  $U = U_e^\dagger U_\nu$  and  $U_\nu = U_T$ , the matrices  $P'_e$  and  $P'_\nu$  are now given by

$$P'_\nu = U^\dagger d_e^2 U + 3 d_T^2, \quad P'_e = 3 d_e^2 + 3 U d_T^2 U^\dagger. \quad (4.4)$$

In order to obtain the RGEs for the mixing angles and CP-violating phases, we adopt the following parameterisation for  $U$ :

$$U = K_\varphi V K_\alpha, \quad K_\varphi = \text{diag}(e^{i\varphi_e}, e^{i\varphi_\mu}, e^{i\varphi_\tau}), \quad K_\alpha = \text{diag}(e^{-i\alpha_1/2}, e^{-i\alpha_2/2}, 1), \quad (4.5)$$

where  $\varphi_{e,\tau,\mu}$  are unphysical phases and  $\alpha_{1,2}$  are CP-violating Majorana phases. The unitary matrix  $V$  is parameterized in the standard way

$$V = \begin{pmatrix} c_{12}c_{13} & s_{12}c_{13} & s_{13}e^{-i\delta} \\ -s_{12}c_{23} - c_{12}s_{23}s_{13}e^{i\delta} & c_{12}c_{23} - s_{12}s_{23}s_{13}e^{i\delta} & s_{23}c_{13} \\ s_{12}s_{23} - c_{12}c_{23}s_{13}e^{i\delta} & -c_{12}s_{23} - s_{12}c_{23}s_{13}e^{i\delta} & c_{23}c_{13} \end{pmatrix}, \quad (4.6)$$

where  $c_{ij} \equiv \cos \theta_{ij}$ ,  $s_{ij} \equiv \sin \theta_{ij}$  and  $\delta$  is the Dirac CP-violating phase. We identify the mixing angles  $\theta_{12}$  and  $\theta_{23}$  as being the ones involved in the solar and atmospheric neutrino oscillations, respectively, while  $\theta_{13}$  denotes the so-called CHOOZ or reactor neutrino mixing angle.

Although physical observables do not depend on the phases  $\varphi_i$ , these are crucial to obtain the RGEs for the physical neutrino parameters (see discussion in ref. [50]). From (3.10) and (4.5) we obtain

$$i \text{diag}(\dot{\varphi}_e, \dot{\varphi}_\mu, \dot{\varphi}_\tau) V + \dot{V} - \frac{i}{2} V \text{diag}(\dot{\alpha}_1, \dot{\alpha}_2, 0) = -\widehat{Q} V + V \widehat{R}, \quad (4.7)$$

which can be used to extract the RGEs for the mixing angles and phases. In the above equation, the matrices  $\widehat{Q}$  and  $\widehat{R}$  are defined by  $\widehat{Q} = K_\varphi^* Q K_\varphi$  and  $\widehat{R} = K_\alpha R K_\alpha^*$ . Together with eqs. (3.6) and (3.8), this leads to

$$16\pi^2 \widehat{Q}_{ij} = (\widehat{P}_e)_{ij} \frac{y_{e_i}^2 + y_{e_j}^2}{y_{e_j}^2 - y_{e_i}^2} \quad (i \neq j), \quad (4.8)$$

$$16\pi^2 \widehat{R}_{ij} = \frac{m_i^2 + m_j^2}{m_j^2 - m_i^2} (\widehat{P}_\nu)_{ij} + \frac{2 m_i m_j}{m_j^2 - m_i^2} (\tilde{P}_\nu)_{ij} \quad (i \neq j), \quad (4.9)$$

where

$$\widehat{P}_e = K_\varphi^* P'_e K_\varphi = 3 d_e^2 + 3 V d_T^2 V^\dagger, \quad (4.10)$$

$$\widehat{P}_\nu = K_\alpha P'_\nu K_\alpha^* = V^\dagger d_e^2 V + 3 d_T^2, \quad (4.11)$$

$$\widetilde{P}_\nu = K_\alpha (P'_\nu)^* K_\alpha^* = K_\alpha^2 V^T d_e^2 V^* K_\alpha^{*2} + 3 d_T^2. \quad (4.12)$$

The above results show that the RGE for the mixing matrix  $U$  does not depend on the unphysical phases  $\varphi_{e,\mu,\tau}$ , as expected. Comparing the present model with the MSSM, it becomes clear that the new contribution to the running of the neutrino mixing matrix comes from the first term on the right-hand side of eq. (4.7), i.e. from the effect of the non-trivial running of  $U_e$  induced by the presence of the couplings  $Y_T$ .

At this point we would like to point out some discrepancies between our results and those obtained in ref. [27].

1. In ref. [27] it is claimed that the RGEs for the mixing angles and CP-violating phases are independent of the Majorana phases  $\alpha_{1,2}$  at any scale  $\Lambda > M_T$ . This is actually not the case, as can be seen from eq. (4.7). Although the first term on the right-hand side of this equation does not depend on  $\alpha_{1,2}$ , the second term does (through the contribution of the term proportional to  $\widetilde{P}$  in  $\widehat{R}$ ). In fact, the dependence of the RGE of  $U$  on  $\alpha_{1,2}$  originates from the running of the effective neutrino mass matrix, more specifically from the term proportional to  $Y_e^\dagger Y_e$  in eq. (2.12). On the other hand,  $\widehat{Q}$  is independent of the Majorana phases since it is defined by  $\widehat{P}_e$  (which does not depend on  $\alpha_{1,2}$ ) and the charged-lepton Yukawa couplings. Hence,  $\dot{U}_e$  does not show any direct dependence on  $\alpha_{1,2}$ .
2. Our results for the TMSSM RGEs agree with the ones of refs. [28] and [29]. However, we find several discrepancies with those obtained in ref. [27] where the conventions for the couplings entering in  $W_T$  are the same as the ones we are currently adopting. We find that, in order to get complete agreement between all results, the couplings  $\lambda_{1,2}$  and  $Y_T$  must be replaced by  $\sqrt{2}\lambda_{1,2}$  and  $\sqrt{2}Y_T$  in all the RGEs of ref. [27], including the one for the effective neutrino mass matrix. This affects the numerical pre-factors in the second term of the right-hand side of eqs. (4.10)–(4.12), which in our case differ by a factor of two from those of ref. [27]. The same holds for all the terms proportional to  $|\lambda_{1,2}|^2$  appearing in eqs. (2.13) and (3.5). We believe that these discrepancies might be the result of an inconsistent definition of the Feynman rules used in ref. [27] for the vertices involving the triplet states.

#### 4.1 RGEs for the neutrino masses, mixing angles and CP-violating phases

We can now use the master equation (4.7) to obtain the RGEs for the mixing angles  $\theta_{ij}$  and CP-violating phases. For each  $\theta_{ij}$  we write the corresponding RGE in the form:

$$\dot{\theta}_{ij} = \dot{\theta}_{ij}^\nu + \dot{\theta}_{ij}^e, \quad \dot{\theta}_{ij}^\nu = \sum_{b>a} \text{Re} \left[ A_{ij}^{ab} \widehat{R}_{ab} \right], \quad \dot{\theta}_{ij}^e = \sum_{b>a} \text{Re} \left[ B_{ij}^{ab} \widehat{Q}_{ab} \right], \quad a, b = 1, 2, 3, \quad (4.13)$$

$ij$	$A_{ij}^{12}$	$A_{ij}^{13}$	$A_{ij}^{23}$
12	1	$s_{12} \tan \theta_{13} e^{i\delta}$	$-c_{12} \tan \theta_{13} e^{i\delta}$
13	0	$c_{12} e^{i\delta}$	$s_{12} e^{i\delta}$
23	0	$-\frac{s_{12}}{c_{13}}$	$\frac{c_{12}}{c_{13}}$
$ij$	$B_{ij}^{12}$	$B_{ij}^{13}$	$B_{ij}^{23}$
12	$-\frac{c_{23}}{c_{13}}$	$\frac{s_{23}}{c_{13}}$	0
13	$-s_{23} e^{i\delta}$	$-c_{23} e^{i\delta}$	0
23	$c_{23} \tan \theta_{13} e^{i\delta}$	$-s_{23} \tan \theta_{13} e^{i\delta}$	-1

**Table 1.** Coefficients  $A_{ij}^{ab}$  (first three rows) and  $B_{ij}^{ab}$  (last three rows) which enter the definition of the RGEs for the mixing angles  $\theta_{ij}$ , given in eq. (4.13).

where  $\dot{\theta}_{ij}^\nu$  and  $\dot{\theta}_{ij}^e$  contain the contributions coming from the running of  $m_\nu$  and  $Y_e$ , respectively. The coefficients  $A_{ij}^{ab}$  and  $B_{ij}^{ab}$  (shown in table 1) are determined by solving eq. (4.7). Similarly, for the full set of phases  $\Phi = (\delta, \alpha_1, \alpha_2, \varphi_e, \varphi_\mu, \varphi_\tau)$ ,

$$\dot{\Phi} = \dot{\Phi}^\nu + \dot{\Phi}^e, \quad \dot{\Phi}^\nu = \sum_{b>a} \text{Im} \left[ A_\Phi^{ab} \widehat{R}_{ab} \right], \quad \dot{\Phi}^e = \sum_{b>a} \text{Im} \left[ B_\Phi^{ab} \widehat{Q}_{ab} \right], \quad a, b = 1, 2, 3, \quad (4.14)$$

where  $\dot{\Phi}^\nu$  and  $\dot{\Phi}^e$  include the terms stemming from  $\dot{m}_\nu$  and  $\dot{Y}_e$ . The coefficients  $A_\Phi^{ab}$  and  $B_\Phi^{ab}$  are given in table 2. Regarding the neutrino masses  $m_i$ , the RGEs can be obtained replacing  $P'_\nu$  by  $\widehat{P}_\nu$  in eq. (3.11), leading to:

$$16\pi^2 \dot{m}_i = \left[ \alpha_\nu + 2 \left( V^\dagger d_e^2 V \right)_{ii} + 6 y_i^2 \right] m_i. \quad (4.15)$$

As expected,  $\dot{m}_i$  does not depend on the Majorana phases  $\alpha_{1,2}$ . Moreover, the third term on the right-hand side of the above equation is independent of the neutrino mixing angles and CP-violating phases. In contrast, the second term (also present in the MSSM case) does depend on those quantities.

The complete expressions for the RGEs of the neutrino mixing angles and phases can be obtained by inserting the coefficients given in tables 1 and 2 into eqs. (4.13) and (4.14), respectively. In general, the final result is too lengthy to be presented here. However, following the procedure of ref. [50], we will expand the RGEs to the leading order in the (small) mixing angle  $\theta_{13}$ . Let us first concentrate on the neutrino contribution to the RGEs of the mixing angles, i.e. the terms  $\dot{\theta}_{ij}^\nu$  in eq. (4.13). These depend on  $V$ , on the neutrino masses and on the charged-lepton Yukawa couplings  $y_{e_i}^2$ . In view of the strong hierarchy  $y_e \ll y_\mu \ll y_\tau$ , we will keep only the terms proportional to  $y_\tau^2$ . In this limit, and in the

$\Phi$	$A_{\Phi}^{12}$	$A_{\Phi}^{13}$	$A_{\Phi}^{23}$
$\delta$	$\frac{1}{c_{12}s_{12}}$	$-\frac{s_{12}V_{22}}{c_{13}c_{12}s_{23}} - \frac{V_{22}^*e^{i\delta}}{s_{13}c_{13}c_{23}}$	$\frac{V_{21}^*e^{i\delta}}{s_{13}c_{13}c_{23}} - \frac{c_{12}V_{21}}{c_{13}s_{12}s_{23}}$
$\alpha_1$	$2 \cot \theta_{12}$	$\frac{2V_{31}}{c_{13}c_{23}} + \frac{2V_{21}}{c_{13}s_{23}}$	$\frac{2V_{32}}{c_{13}c_{23}} - \frac{2c_{12}V_{21}}{c_{13}s_{23}s_{12}}$
$\alpha_2$	$2 \tan \theta_{12}$	$\frac{2V_{31}}{c_{13}c_{23}} - \frac{2s_{12}V_{22}}{c_{13}s_{23}c_{12}}$	$\frac{2V_{32}}{c_{13}c_{23}} + \frac{2V_{22}}{c_{13}s_{23}}$
$\varphi_e$	$\frac{1}{c_{12}s_{12}}$	$\frac{V_{31}}{c_{13}c_{23}} - \frac{s_{12}V_{22}}{c_{13}s_{23}c_{12}}$	$\frac{V_{32}}{c_{13}c_{23}} - \frac{c_{12}V_{21}}{c_{13}s_{23}s_{12}}$
$\varphi_{\mu}$	0	$\frac{V_{22}}{c_{13}s_{23}}$	$\frac{V_{21}}{c_{13}s_{23}}$
$\varphi_{\tau}$	0	$\frac{V_{31}}{c_{13}c_{23}}$	$\frac{V_{32}}{c_{13}c_{23}}$
$\Phi$	$B_{\Phi}^{12}$	$B_{\Phi}^{13}$	$B_{\Phi}^{23}$
$\delta$	$\frac{c_{23}V_{32}}{c_{13}s_{12}s_{23}} - \frac{V_{32}^*e^{i\delta}}{s_{13}c_{12}c_{13}}$	$-\frac{s_{23}V_{21}}{c_{23}c_{12}c_{13}} - \frac{V_{21}^*e^{i\delta}}{s_{13}c_{13}s_{12}}$	$-\frac{1}{s_{23}c_{23}}$
$\alpha_1$	$\frac{2c_{23}V_{32}}{s_{12}c_{13}s_{23}}$	$\frac{2s_{23}V_{22}}{s_{12}c_{13}c_{23}}$	$-\frac{2}{s_{23}c_{23}}$
$\alpha_2$	$\frac{2c_{23}V_{31}}{c_{12}c_{13}s_{23}}$	$\frac{2s_{23}V_{21}}{c_{12}c_{13}c_{23}}$	$-\frac{2}{s_{23}c_{23}}$
$\varphi_e$	$\frac{c_{23}V_{32}}{s_{12}s_{23}c_{13}} - \frac{V_{21}}{c_{13}c_{12}}$	$\frac{s_{23}V_{22}}{s_{12}c_{23}c_{13}} - \frac{V_{31}}{c_{13}c_{12}}$	$-\frac{1}{s_{23}c_{23}}$
$\varphi_{\mu}$	$-\frac{V_{13}^*}{c_{13}s_{23}}$	0	$-\cot \theta_{23}$
$\varphi_{\tau}$	0	$-\frac{V_{13}^*}{c_{13}c_{23}}$	$\tan \theta_{13}$

**Table 2.** Coefficients  $A_{\Phi}^{ab}$  (first six rows) and  $B_{\Phi}^{ab}$  (last six rows) which enter the definition of the RGEs for the CP-violating phases  $\Phi = (\delta, \alpha_1, \alpha_2, \varphi_e, \varphi_{\mu}, \varphi_{\tau})$  given in eq. (4.14).

zeroth order in  $\theta_{13}$ , we find

$$\begin{aligned}
 \dot{\theta}_{13}^{\nu} &\simeq -\frac{y_{\tau}^2}{32\pi^2} \frac{m_3}{\Delta m_{31}^2} \sin(2\theta_{23}) \sin(2\theta_{12}) \left[ -m_1 \cos(\alpha_1 - \delta) + \frac{m_2 \cos(\alpha_2 - \delta)}{(1-r)} + \frac{r m_3 \cos \delta}{(1-r)} \right], \\
 \dot{\theta}_{12}^{\nu} &\simeq -\frac{y_{\tau}^2}{32\pi^2} \frac{|m_1 e^{i\alpha_1} + m_2 e^{i\alpha_2}|^2}{r \Delta m_{31}^2} s_{23}^2 \sin(2\theta_{12}), \\
 \dot{\theta}_{23}^{\nu} &\simeq -\frac{y_{\tau}^2}{32\pi^2} \left[ c_{12}^2 \frac{|m_3 + m_2 e^{i\alpha_2}|^2}{\Delta m_{31}^2 (1-r)} + s_{12}^2 \frac{|m_1 + m_3 e^{i\alpha_1}|^2}{\Delta m_{31}^2} \right] \sin(2\theta_{23}),
 \end{aligned} \tag{4.16}$$

where

$$r = \frac{\Delta m_{21}^2}{\Delta m_{31}^2}, \quad \Delta m_{ij}^2 \equiv m_j^2 - m_i^2. \tag{4.17}$$

The above expressions make explicit the discrepancies between our results and those of ref. [27]. From eqs. (4.16) it is clear that the running of the neutrino mixing angles *does depend* on the Majorana phases through the renormalisation of the effective neutrino mass matrix  $m_{\nu}$ . The above contributions to the RGEs originate from the wave-function renormalisation of the lepton doublets, namely from the term proportional to  $Y_e^{\dagger} Y_e$ , present below and above the decoupling scale of the triplets. Therefore, eqs. (4.16) are valid both in the effective and in the full theory. Not surprisingly, the results for  $\dot{\theta}_{ij}^{\nu}$  agree with those obtained for the MSSM in ref. [50]. Hence, the expansions given in ref. [27] are *not valid* above the mass scale of the triplets since they do not account for the dependence of the

RG running on the Majorana phases, which may play a crucial rôle in the running of the neutrino parameters.

The approximate expressions for the RGEs of the Majorana phases  $\alpha_{1,2}$  read

$$\dot{\alpha}_1^\nu \simeq -\frac{y_\tau^2}{4\pi^2} \left\{ \frac{m_1 m_2 s_{23}^2 c_{12}^2}{r \Delta m_{31}^2} \sin(\alpha_1 - \alpha_2) + \frac{m_3 \cos(2\theta_{23})}{\Delta m_{31}^2} \left[ m_1 s_{12}^2 s_{\alpha_1} + \frac{m_2 c_{12}^2 s_{\alpha_2}}{(1-r)} \right] \right\}, \quad (4.18)$$

$$\dot{\alpha}_2^\nu \simeq -\frac{y_\tau^2}{4\pi^2} \left\{ \frac{m_1 m_2 s_{23}^2 s_{12}^2}{r \Delta m_{31}^2} \sin(\alpha_1 - \alpha_2) + \frac{m_3 \cos(2\theta_{23})}{\Delta m_{31}^2} \left[ m_1 s_{12}^2 s_{\alpha_1} + \frac{m_2 c_{12}^2 s_{\alpha_2}}{(1-r)} \right] \right\}, \quad (4.19)$$

in contrast with the result  $\dot{\alpha}_{1,2}^\nu \simeq 0$  obtained in ref. [27] at zeroth order in  $\theta_{13}$ . There, the lowest-order term in the expansion of  $\dot{\alpha}_{1,2}$  was found to be of first order in  $\theta_{13}$ , giving rise to the conclusion that the RG effects on  $\alpha_{1,2}$  are small. The reason why the above terms were not obtained in [27] has to do with the fact that they vanish for  $\alpha_{1,2} = 0$ , which is the only limit in which the expressions given in that reference are valid.

The neutrino contribution to the RGE of the Dirac CP-violating phase  $\delta$  can be expressed in the form [50]

$$\dot{\delta}^\nu = \frac{y_\tau^2}{32\pi^2} \frac{\dot{\delta}_{(-1)}^\nu}{\theta_{13}} + \frac{y_\tau^2}{8\pi^2} \dot{\delta}_{(0)}^\nu, \quad (4.20)$$

where  $\dot{\delta}_{(-1)}^\nu$  and  $\dot{\delta}_{(0)}^\nu$  are given by

$$\dot{\delta}_{(-1)}^\nu = \frac{m_3 \sin(2\theta_{12}) \sin(2\theta_{23})}{\Delta m_{31}^2} \left[ m_1 \sin(\alpha_1 - \delta) + m_2 \frac{\sin(\alpha_2 - \delta)}{1-r} + \frac{r m_3}{1-r} \sin \delta \right], \quad (4.21)$$

$$\begin{aligned} \dot{\delta}_{(0)}^\nu &= \frac{m_1 m_2 s_{23}^2}{r \Delta m_{31}^2} \sin(\alpha_1 - \alpha_2) + \frac{m_3 \cos(2\theta_{23})}{\Delta m_{31}^2} \left[ m_1 s_{12}^2 \sin \alpha_1 + \frac{m_2 c_{12}^2 \sin \alpha_2}{1-r} \right] + \\ &+ \frac{m_3 c_{23}^2}{\Delta m_{31}^2} \left[ m_1 c_{12}^2 \sin(2\delta - \alpha_1) + \frac{m_2}{1-r} s_{12}^2 \sin(2\delta - \alpha_2) \right]. \end{aligned} \quad (4.22)$$

Again, this differs from ref. [27] since  $\dot{\delta}_{(0)}^\nu$  does not vanish (even in the limit of vanishing Majorana phases) and  $\dot{\delta}_{(-1)}^\nu$  does depend on  $\alpha_{1,2}$ . In the limit  $\alpha_{1,2} = 0$ , our result for  $\dot{\delta}_{(-1)}^\nu$  agrees with the one of [27].

Let us now consider the charged-lepton contribution to the RGEs of the mixing angles and CP-violating phases denoted by  $\dot{\theta}_{ij}^e$  and  $\dot{\Phi}_i^e$  in eqs. (4.13) and (4.14). At zeroth order in  $\theta_{13}$  we obtain

$$\dot{\theta}_{12}^e \simeq \frac{3r \Delta m_{31}^2}{32\pi^2 v_T^2} \frac{y_e^4 - y_\mu^2 y_\tau^2 + y_e^2 (y_\mu^2 - y_\tau^2) \cos(2\theta_{23})}{(y_\mu^2 - y_e^2)(y_\tau^2 - y_e^2)} \sin(2\theta_{12}) \simeq -\frac{3r \Delta m_{31}^2}{32\pi^2 v_T^2} \sin(2\theta_{12}), \quad (4.23)$$

$$\dot{\theta}_{23}^e \simeq -\frac{3\Delta m_{31}^2}{32\pi^2 v_T^2} \frac{y_\mu^2 + y_\tau^2}{y_\tau^2 - y_\mu^2} (1 - r c_{12}^2) \sin(2\theta_{23}) \simeq -\frac{3\Delta m_{31}^2}{32\pi^2 v_T^2} (1 - r c_{12}^2) \sin(2\theta_{23}), \quad (4.24)$$

$$\dot{\theta}_{13}^e \simeq -\frac{3r \Delta m_{31}^2}{32\pi^2 v_T^2} \frac{y_e^2 (y_\tau^2 - y_\mu^2)}{(y_\mu^2 - y_e^2)(y_\tau^2 - y_e^2)} \sin(2\theta_{12}) \sin(2\theta_{23}) \cos \delta \simeq 0, \quad (4.25)$$

where the final results correspond to the limit  $y_{e,\mu} \rightarrow 0$ . For the Majorana phases we find  $\dot{\alpha}_{1,2}^e \simeq 0$ , at zeroth order in  $\theta_{13}$ , while for  $\dot{\delta}^e$  we have

$$\dot{\delta}^e \simeq \frac{3r \Delta m_{31}^2}{32\pi^2 v_T^2} \frac{y_e^2 (y_\tau^2 - y_\mu^2)}{(y_\mu^2 - y_e^2)(y_\tau^2 - y_e^2)} \theta_{13}^{-1} \sin(2\theta_{12}) \sin(2\theta_{23}) \sin \delta. \quad (4.26)$$

Comparing our results for the charged-lepton contribution to the running of the mixing angles and CP-phases (in the  $y_{e,\mu} \rightarrow 0$  limit) with those of ref. [27], we find a general agreement. The only difference, which is the consequence of the discrepancies in the RGE of  $Y_e$  (see the paragraph preceding section 4.1), is the overall factor of 3 in eqs. (4.23)–(4.26) which replaces the factor of 3/2 of [27].

From eqs. (4.23)–(4.25) one immediately concludes that  $\dot{\theta}_{12,13}^e$  are mainly controlled by the factor  $r\Delta m_{31}^2/v_T^2 = y_2^2 - y_1^2$ , with  $\dot{\theta}_{13}^e$  further suppressed by  $y_e^2/y_\mu^2 \ll 1$ . On the other hand,  $\dot{\theta}_{23}^e$  is essentially governed by  $\Delta m_{31}^2/v_T^2 = y_3^2 - y_1^2$ . Therefore, since  $r$  is small we expect larger RG effects on  $\theta_{23}$  than on the remaining mixing angles. This is in contrast with what happens for the contributions  $\dot{\theta}_{ij}^\nu$  shown in (4.16), where the running is typically enhanced for  $\theta_{12}$  with respect to  $\theta_{13,23}$  due to an  $1/r$  factor present in  $\dot{\theta}_{12}^\nu$ . Since the overall signs of  $\dot{\theta}_{12,23}^\nu$  and  $\dot{\theta}_{12,23}^e$  are the same, both the neutrino and charged-lepton contributions to  $\dot{\theta}_{12,23}$  tend to affect the RG flow of these mixing angles in the same way. As for the running of  $\theta_{13}$ , the main contribution to  $\dot{\theta}_{13}$  comes from  $\dot{\theta}_{13}^\nu$  which, for a given value of  $m_i$ , may be positive or negative depending on the values of  $\alpha_{1,2}$  and  $\delta$ .

The RGEs for the neutrino masses  $m_i$  and the charged-lepton Yukawa couplings  $y_{e_i}$  can be obtained from eqs. (3.11) and (3.12) with  $\alpha_\nu$ ,  $\alpha_e$  and  $P'_{\nu,e}$  given as in (2.14), (3.5) and (4.4), respectively. Here we focus on the running of the parameter  $r$  defined in (4.17). The value of  $r$  is crucial in model building since, although not affected by overall factors in the effective neutrino mass matrix, it is sensitive to the flavour structure of  $m_\nu$ . At low energies  $|r(m_Z)| \simeq 0.03$  (see section 4.2).

We consider two types of neutrino mass spectra,

$$\text{Normally – ordered (NO) : } m_1 < m_2 < m_3, \tag{4.27}$$

$$\text{Inversely – ordered (IO) : } m_3 < m_1 < m_2, \tag{4.28}$$

in such a way that  $r$  is positive (negative) for the NO (IO) case. Using eqs. (2.14), (3.11) and (4.4), we can write the RGE for  $r$  as:<sup>5</sup>

$$\text{NO : } 4\pi^2\dot{r} = -r\Delta P'_{32} + \frac{m_1^2}{\Delta m_{31}^2} (\Delta P'_{21} - r\Delta P'_{31}), \tag{4.29}$$

$$\text{IO : } 4\pi^2\dot{r} = \Delta P'_{21}(r - 1) + \frac{m_3^2}{\Delta m_{31}^2} (\Delta P'_{21} - r\Delta P'_{31}), \tag{4.30}$$

with  $\Delta P'_{ij} \equiv (P'_\nu)_{ii} - (P'_\nu)_{jj}$ . To better distinguish the two main sources of RG effects, we express  $\dot{r}$  in the form:

$$r = \dot{r}_e + \dot{r}_T, \tag{4.31}$$

where  $\dot{r}_e$  and  $\dot{r}_T$  denote the terms depending on the charged-lepton and  $Y_T$  Yukawa couplings  $y_{e_i}$  and  $y_i$ , respectively. The contributions  $\dot{r}_e$  originate from the first term of  $P'_\nu$  (see eq. (4.4)) and therefore will depend on  $y_{e,\mu,\tau}^2$  and on the neutrino mixing parameters. At leading order in  $\theta_{13}$  (and keeping only the terms proportional to  $y_\tau^2$ ), we obtain for both

---

<sup>5</sup>Notice that the following equations are equivalent to each other. We choose to write them differently for the NO and IO cases to better identify the terms which are proportional to  $m_{1,3}^2/\Delta m_{31}^2$ .

Parameter	Best-fit	$3\sigma$
$\Delta m_{21}^2$ [ $10^{-5}$ eV $^2$ ]	$7.65^{+0.23}_{-0.20}$	7.05–8.34
$ \Delta m_{31}^2 $ [ $10^{-3}$ eV $^2$ ]	$2.40^{+0.12}_{-0.11}$	2.07–2.75
$\sin^2 \theta_{12}$	$0.304^{+0.022}_{-0.016}$	0.25–0.37
$\sin^2 \theta_{23}$	$0.50^{+0.07}_{-0.06}$	0.36–0.67
$\sin^2 \theta_{13}$	$0.01^{+0.016}_{-0.011}$	$\leq 0.056$
$ r $	0.032	0.027–0.038

**Table 3.** Best-fit values (with  $1\sigma$  errors) and  $3\sigma$  allowed intervals for the neutrino oscillation parameters from global data including solar, atmospheric, reactor (KamLAND and CHOOZ) and accelerator (K2K and MINOS) experiments [10].

the NO and IO neutrino mass spectra:

$$\text{NO} : \dot{r}_e = -\frac{y_\tau^2}{16\pi^2} \left\{ \frac{m_1^2}{\Delta m_{31}^2} [r + 3r \cos(2\theta_{23}) - 2(2-r) \cos(2\theta_{12})s_{23}^2] + r [1 + 3 \cos(2\theta_{23}) - 2 \cos(2\theta_{12})s_{23}^2] \right\}, \quad (4.32)$$

$$\text{IO} : \dot{r}_e = -\frac{y_\tau^2}{16\pi^2} \left\{ \frac{m_3^2}{\Delta m_{31}^2} [r + 3r \cos(2\theta_{23}) - 2(2-r) \cos(2\theta_{12})s_{23}^2] + 4(1-r)s_{23}^2 \cos(2\theta_{12}) \right\}. \quad (4.33)$$

It is worth noticing that in the limit of quasi-degenerate neutrinos ( $m_1 \simeq m_2 \simeq m_3 \gg \Delta m_{31}^2$ ) and/or large  $\tan \beta$ , the RG effects on  $r$  due to  $\dot{r}_e$  are enhanced. For hierarchical (HI) neutrino masses (NO with  $m_1 \ll \Delta m_{21}^2$ ), we do not expect major effects due to the suppression factor of  $r$  present in the second term of (4.32). Yet, in the inverted-hierarchical (IH) situation (IO with  $m_3 \ll \Delta m_{21}^2$ ) there is an unsuppressed term in eq. (4.33) which, depending on the value of  $\tan \beta$ , may lead to a considerable running of  $r$ .

The remaining contribution to  $\dot{r}$  (denoted by  $\dot{r}_T$  in eq. (4.31)) does not depend directly on the neutrino mixing angles since it originates from the second term of  $P'_\nu$ , which is diagonal. From eqs. (4.29) we obtain

$$\dot{r}_T = -\frac{3(y_3^2 - y_1^2)}{4\pi^2} r(1-r) = -\frac{3\Delta m_{31}^2}{4\pi^2 v_T^2} r(1-r), \quad (4.34)$$

for both the NO and IO cases. Contrarily to the results obtained for  $\dot{r}_e$ , the above equation is exact in the sense that it does not rely on any expansion nor on any special limit of the couplings. An immediate conclusion that can be drawn from (4.34) is that, although  $\dot{r}_T$  is always negative,  $|r|$  decreases (increases) when going from low to high energies, for a NO (IO) neutrino mass spectrum. Clearly, this is only true in the limit of negligible  $\dot{r}_e$ .

## 4.2 Numerical examples

At low energies, the neutrino mixing angles and mass squared differences are constrained by solar, atmospheric, reactor (KamLAND and CHOOZ) and accelerator (K2K and MINOS) neutrino oscillation experiments. The results of a global analysis [10] of the data provided



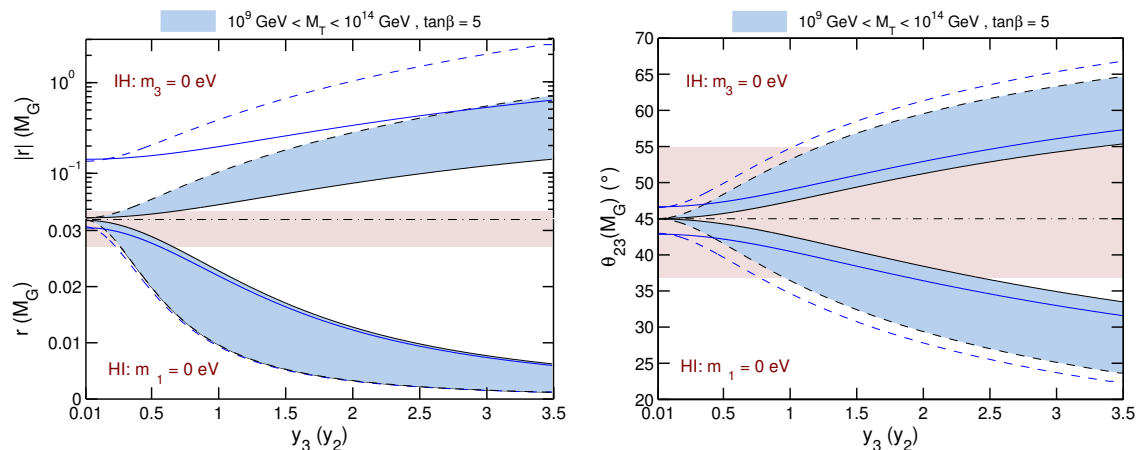


**Figure 2.** Left plot: Values of  $r$  and  $|r|$  at  $\Lambda = M_G$  for the HI (lower branch) and IH (upper branch) cases as a function of the largest  $y_i$  coupling ( $y_3$  for HI and  $y_2$  IH). The blue-filled regions correspond to the variation of  $r$  and  $|r|$  in the interval  $M_T = 10^9$  GeV (black-dashed line) to  $10^{14}$  GeV (black-solid line) and  $\tan\beta = 5$ . The blue-solid (dashed) line shows the result for  $\tan\beta = 50$  and  $M_T = 10^9$  ( $10^{14}$ ) GeV. The horizontal pink bar denotes the low-energy  $3\sigma$  allowed range for  $|r|$  as given in table 3, while the best-fit value is indicated by the horizontal dash-dotted line. Right plot: the same as in the left plot but for the mixing angle  $\theta_{23}$ . For both plots we used  $\theta_{13}(m_Z) = 0$  and the best-fit values for the remaining parameters ( $\theta_{12}$ ,  $\theta_{23}$ ,  $\Delta m_{21}^2$  and  $|\Delta m_{31}^2|$ ). All CP-violating phases are set to zero.

by these experiments are summarised in table 3 where the best-fit values and  $3\sigma$  intervals for  $\theta_{ij}$ ,  $\Delta m_{21}^2$  and  $|\Delta m_{31}^2|$  (as well as for  $|r|$ ) are presented.

In the following, we will show some numerical examples with the aim of quantifying the RG effects on the neutrino mass and mixing parameters due to the presence of the heavy triplets  $T$  and  $\bar{T}$ . We adopt the bottom-up approach, i.e. we start at  $\Lambda = m_Z$  with the best-fit values of the low-energy neutrino parameters and evolve the full set of the MSSM RGEs up to  $\Lambda = M_T$ . At this scale, we extract  $Y_T$  according to eq. (4.1) and run the TMSSM RGEs to the GUT scale  $M_G \simeq 2 \times 10^{16}$  GeV. The RG effects in the neutrino mixing matrix  $U$  and in the neutrino masses  $m_i$  are governed by eqs. (3.10) and (3.11), respectively. We will only consider the cases of HI and IH neutrino mass spectra, for which the contributions to the running coming from the neutrino sector are, in general, suppressed with respect to what happens in the quasi-degenerate limit. In addition, only the results for  $r$  and the mixing angle  $\theta_{23}$  will be shown since, as discussed in the previous section, the RG effects induced by  $Y_T$  are less important for  $\theta_{12,13}$ .

In the lower (upper) part of the left plot in figure 2, we show the values of  $r(M_G)$  ( $|r(M_G)|$ ) as a function of the coupling  $y_3$  ( $y_2$ ) for the HI (IH) case.<sup>6</sup> The triplet-mass  $M_T$  (always given at  $\Lambda = M_T$ ) is varied between  $10^9$  GeV and  $10^{14}$  GeV. These limits correspond to the solid and dashed curves (in black for  $\tan\beta = 5$  and in blue for  $\tan\beta = 50$ ),

<sup>6</sup>The values of  $y_3$  and  $y_2$  (given at  $\Lambda = M_G$ ) are extracted using eqs. (4.3) and taking appropriate ranges for  $\lambda_2$  at each value of  $M_T$ .



respectively. From eqs. (4.31)–(4.34) we obtain for the cases under discussion:

$$\text{HI} : \dot{r} \simeq -\frac{y_\tau^2}{16\pi^2} r \left[ 1 + 3 \cos(2\theta_{23}) - 2 \cos(2\theta_{12}) s_{23}^2 \right] - \frac{3y_3^2}{4\pi^2} r(1-r), \quad (4.35)$$

$$\text{IH} : \dot{r} \simeq -\frac{y_\tau^2}{4\pi^2} (1-r) s_{23}^2 \cos(2\theta_{12}) + \frac{3y_1^2}{4\pi^2} r(1-r). \quad (4.36)$$

For small  $\tan\beta$  and  $y_i \ll 1$  we do not expect large RG running effects on  $r$  since  $\dot{r}_e$  and  $\dot{r}_T$  are suppressed by the small couplings  $y_\tau$  and  $y_i$ . This is true for both the HI and IH cases, as confirmed by the left plot of figure 2. For small  $y_i$  and  $\tan\beta = 5$ , the value of  $r(M_G)$  is very close to  $r(m_Z) = 0.032$  (see table 2), indicated by the horizontal dash-dotted line. As the couplings  $y_i$  increase,  $\dot{r}_T$  increases and  $\dot{r}$  is mainly given by the second term on the right-hand side of eqs. (4.35) and (4.36). As expected,  $r$  decreases from low to high energies for the HI case since  $\dot{r}_T$  is negative and  $r(m_Z) > 0$ . In contrast, although  $\dot{r}_T < 0$  also in the IH limit,  $r(m_Z) < 0$  and therefore  $|r|$  increases when going from  $m_Z$  to  $M_G$ . Notice that for  $y_{3,2} \sim 1$  the value of  $r(M_G)$  is outside the  $3\sigma$  low-energy allowed region even for the largest allowed value of  $M_T$ . In the small  $\tan\beta$  limit, we obtain the following approximate results

$$\text{HI} : r(M_G) \simeq r_0 \left[ r_0 + (1-r_0) \left( \frac{M_G}{M_T} \right)^{\frac{3y_3^2}{4\pi^2}} \right]^{-1} \simeq (9.1 \times 10^{-3}, 2.2 \times 10^{-2}), \quad (4.37)$$

$$\text{IH} : |r(M_G)| \simeq |r_0| \left[ -|r_0| + (1+|r_0|) \left( \frac{M_T}{M_G} \right)^{\frac{3y_1^2}{4\pi^2}} \right]^{-1} \simeq (0.1, 4.9 \times 10^{-2}), \quad (4.38)$$

where  $r_0 \equiv r(m_Z)$ . The numbers in parentheses correspond to the estimates for  $M_T = 10^9$  GeV and  $10^{14}$  GeV, respectively, taking  $y_{3,1} = 1$ .

For the HI case, the large  $\tan\beta$  results are similar to the small  $\tan\beta$  ones, with the RG correction reaching approximately 10% for small values of  $y_i$  and  $\tan\beta = 50$  (blue curves on the lower part of the left plot in figure 2). This correction is small due to the fact that the term proportional to  $y_\tau^2$  in eq. (4.35) is suppressed by  $r$ . Instead, a large effect is observed in the IH limit with large  $\tan\beta$  since the first term in eq. (4.36) is not suppressed by  $r$ . Therefore, in this case the contribution proportional to  $y_\tau^2$  is important even for small values of  $y_2$ . We find  $|r(M_G)| \simeq 0.2$  for  $y_2 \ll 1$  and  $\tan\beta = 50$ .

Let us now turn to the RG effects to  $\theta_{23}$ . From eqs. (4.16) and (4.24) we obtain

$$\text{HI} : \dot{\theta}_{23} \simeq -\frac{y_\tau^2}{32\pi^2} \frac{1 - r \cos(2\theta_{12}) + 2c_{12}^2 \sqrt{r}}{1-r} \sin(2\theta_{23}) - \frac{3y_3^2}{32\pi^2} (1 - rc_{12}^2) \quad (4.39)$$

$$\text{IH} : \dot{\theta}_{23} \simeq \frac{y_\tau^2}{32\pi^2} \sin(2\theta_{23}) + \frac{3y_1^2}{32\pi^2} (1 - rc_{12}^2), \quad (4.40)$$

which show that  $\theta_{23}$  decreases (increases) from low to high energies for the HI (IH) neutrino mass spectrum. This can also be seen in the right plot of figure 2 where  $\theta_{23}(M_G)$  is plotted as a function of  $y_3$  ( $y_2$ ) for the HI (IH) case. When  $y_i \gtrsim 1$  the values of  $\theta_{23}(M_G)$  are outside the  $3\sigma$  low-energy allowed interval for  $\theta_{23}$  (shown in pink). Similarly as for  $r$ , the running

effects are negligible for small  $\tan\beta$  (black solid and dashed curves) and  $y_i \ll 1$ . The value of  $\theta_{23}$  at  $\Lambda = M_G$  can be roughly approximated by

$$\theta_{23}(M_G) \simeq \theta_{23}(m_Z) \mp \frac{m_\tau^2 \tan^2\beta}{32\pi^2 v^2} \ln\left(\frac{M_G}{m_Z}\right) \mp \frac{3y_{3,1}^2}{32\pi^2} \ln\left(\frac{M_G}{M_T}\right), \quad (4.41)$$

where the minus (plus) sign corresponds to the HI (IH) case. As can be seen from the right plot in figure 2, the shape of the curves is nearly the same for different values of  $\tan\beta$ . The results differ due to the second term on the right-hand side of eq. (4.41), which increases (in absolute value) with increasing  $\tan\beta$ . Notice that the overall sign of that term is negative (positive) for the HI (IH) case, which explains the downward (upward) displacement of the  $\tan\beta = 50$  curves with respect to the  $\tan\beta = 5$  ones.

## 5 LFV $\ell_i \rightarrow \ell_j \gamma$ decays in the TMSSM

The observation of lepton-flavour violating processes like  $\ell_i \rightarrow \ell_j \gamma$  would definitely point towards the existence of new sources of lepton flavour violation and/or new physics close to the electroweak scale. So far, none of the aforementioned processes has been observed. The current upper bounds for their branching ratios (BRs) are:

$$\text{BR}(\mu \rightarrow e \gamma) \leq 1.2 \times 10^{-11} \quad [51], \quad (5.1)$$

$$\text{BR}(\tau \rightarrow e \gamma) \leq 1.1 \times 10^{-7} \quad [52] \quad (9.4 \times 10^{-8}), \quad (5.2)$$

$$\text{BR}(\tau \rightarrow \mu \gamma) \leq 4.5 \times 10^{-8} \quad [53] \quad (1.6 \times 10^{-8}), \quad (5.3)$$

where the numbers in parentheses report the results for the  $\tau$  decays obtained through a combined analysis of BABAR and Belle data [54].

The above limits severely constrain the MSSM LFV soft SUSY-breaking mass matrices forcing them to be small. In the slepton sector, flavour violation can be generated in the presence of superpotential renormalisable interactions through RG effects. The most typical example is having the off-diagonal slepton masses arising due to the Dirac neutrino Yukawa couplings which participate in the type I seesaw mechanism of neutrino mass generation [30]. In spite of the huge amount of work done in the direction of establishing a direct connection between low-energy neutrino data and lepton-flavour violation in the SUSY type I seesaw, such goal cannot be achieved in a model-independent way (for a discussion see e.g. ref. [57]). This stems from the impossibility of reconstructing the high-energy neutrino couplings from low-energy neutrino data. In the triplet-seesaw case the situation is improved since the effective neutrino mass matrix is linear on the couplings  $Y_T$  (see eq. (4.1)) and therefore, in general, the flavour structure of  $m_\nu$  is the same as the one of  $Y_T$ .

### 5.1 Approximate predictions for the $\ell_i \rightarrow \ell_j \gamma$ rates

Let us consider the slepton soft SUSY-breaking lagrangian,

$$\mathcal{L}_{\text{soft}} = \tilde{L}^\dagger m_{\tilde{L}}^2 \tilde{L} + \tilde{e}^c m_{\tilde{e}^c}^2 \tilde{e}^{c\dagger} + (H_1 \tilde{e}^c A_e \tilde{L} + \text{H.c.}), \quad (5.4)$$

where  $m_{\tilde{L}}^2$  and  $m_{\tilde{e}^c}^2$  are the SUSY-breaking masses for the slepton doublets and singlets respectively, and  $A_e$  the trilinear terms. Starting at the scale  $\Lambda > M_T$  with universal

boundary conditions  $m_L^2 = m_{e^c}^2 = m_0^2 \mathbb{1}$  and  $A_e = A_0 Y_e$ , at the scale  $M_T$  one approximately has [28]

$$(m_L^2)_{ij} \simeq -\frac{9m_0^2 + 3A_0^2}{8\pi^2} (Y_T^\dagger Y_T)_{ij} \log \frac{\Lambda}{M_T}, \quad (5.5)$$

$$(m_{e^c}^2)_{ij} \simeq 0, \quad (5.6)$$

$$(A_e)_{ij} \simeq -\frac{9}{16\pi^2} A_0 (Y_e Y_T^\dagger Y_T)_{ij} \log \frac{\Lambda}{M_T}, \quad (5.7)$$

where  $i \neq j$  and  $Y_T$  and  $Y_e$  are taken at the  $M_T$  scale.<sup>7</sup> The above LFV terms may be large enough to generate observable rates for LFV processes like radiative charged-lepton decays  $\ell_i \rightarrow \ell_j \gamma$ . Neglecting small effects of the RG running from  $M_T$  to  $m_Z$  of the LFV entries of  $(m_L^2)$ , the quantities on the left-hand sides of eqs. (5.5)–(5.7) can be identified with their values at low-energies. Assuming that only the LFV coming from  $(m_L^2)_{ij}$  is relevant, and keeping the  $\tan \beta$  enhanced contributions to the one-loop amplitudes, one can roughly approximate  $\text{BR}(\ell_i \rightarrow \ell_j \gamma)$  by

$$\text{BR}(\ell_i \rightarrow \ell_j \gamma) \simeq \frac{48\pi^3 \alpha}{G_F^2} |C_{ij}|^2 \tan^2 \beta \text{BR}(\ell_i \rightarrow \ell_j \nu_i \bar{\nu}_j), \quad (5.8)$$

where  $\alpha$  and  $G_F$  are the fine-structure and Fermi constants, respectively, and  $\text{BR}(\mu \rightarrow e \nu_\mu \bar{\nu}_e) = 0.1737$  and  $\text{BR}(\tau \rightarrow \mu \nu_\tau \bar{\nu}_\mu) = 0.1784$ . The coefficients  $C_{ij}$  summarise the dependence of the  $\ell_i \rightarrow \ell_j \gamma$  decay rate on the LFV entries of the slepton mass matrices and masses of the SUSY particles running in the relevant loop diagrams. In the simplest approximation, one has

$$C_{ij} \sim \frac{g_2^2}{16\pi^2} \frac{(m_L^2)_{ij}}{m_S^4}, \quad (i \neq j = e, \mu, \tau), \quad (5.9)$$

where  $g_2$  is the SU(2) gauge-coupling constant and  $m_S$  denotes a common mass scale for the SUSY particles participating in the process. In general, the above approximations do not provide an accurate result for the value of  $\text{BR}(\ell_i \rightarrow \ell_j \gamma)$ . For this reason, it is convenient to work with ratios of BRs instead of the BRs themselves. We will therefore consider the quantities

$$R_{\tau j} \equiv \frac{\text{BR}(\tau \rightarrow \ell_j \gamma)}{\text{BR}(\mu \rightarrow e \gamma)}, \quad j = e, \mu, \quad (5.10)$$

which in the approximation (5.9) are given by

$$R_{\tau j} \simeq \left| \frac{(m_L^2)_{\tau j}}{(m_L^2)_{\mu e}} \right|^2 \text{BR}(\tau \rightarrow \ell_j \nu_\tau \bar{\nu}_j), \quad (5.11)$$

i.e., depend only on the relative strength of LFV in the different channels.<sup>8</sup> Using the approximate expression for  $(m_L^2)_{ij}$  given in eq. (5.5), the ratios of LFV entries of the

<sup>7</sup>In this approximation the small RG running effects on  $Y_T$  and  $Y_e$  between the scales  $\Lambda$  and  $M_T$  are neglected.

<sup>8</sup>As it will be discussed in the next section, this statement is only valid in the limit of quasi-degenerate masses for the three slepton generations.

slepton mass matrix appearing in eq. (5.11) can be expressed in terms of the couplings  $Y_T$  (taken e.g. at the scale  $M_T$ ) as

$$\left| \frac{(m_{\tilde{L}}^2)_{\tau j}}{(m_{\tilde{L}}^2)_{\mu e}} \right|^2 \simeq \left| \frac{(Y_T^\dagger Y_T)_{\tau j}}{(Y_T^\dagger Y_T)_{\mu e}} \right|. \quad (5.12)$$

Unlike the seesaw type I models,  $Y_T$  at the  $M_T$  or  $\Lambda$  scale can in the TMSSM be uniquely computed if values of the neutrino parameters are specified at  $m_Z$ . In this section, following the common procedure, we will set

$$\left| \frac{(Y_T^\dagger Y_T)_{\tau j}}{(Y_T^\dagger Y_T)_{\mu e}} \right|_{\Lambda=M_T}^2 \simeq \left| \frac{(m_\nu^\dagger m_\nu)_{\tau j}}{(m_\nu^\dagger m_\nu)_{\mu e}} \right|_{\Lambda=m_Z}^2, \quad (5.13)$$

neglecting the RG running of the neutrino mass matrix between  $m_Z$  and  $M_T$ . We will assess the quality of this approximation in the next sections.

We now use eq. (3.1) and the parameterisation of the mixing matrix  $V$  adopted in (4.5) and (4.6) to express  $(m_{\tilde{L}}^2)_{ij}$  in terms of the low-energy neutrino parameters:

$$|(m_{\tilde{L}}^2)_{\mu e}|^2 \propto \frac{|\Delta m_{31}^2|}{4v_T^2} c_{13}^2 [r^2 c_{23}^2 \sin^2(2\theta_{12}) + a^2 s_{13}^2 s_{23}^2 + a|r|s_{13}c_\delta \sin(2\theta_{12}) \sin(2\theta_{23})], \quad (5.14)$$

$$|(m_{\tilde{L}}^2)_{\tau e}|^2 \propto \frac{|\Delta m_{31}^2|}{4v_T^2} c_{13}^2 [r^2 s_{23}^2 \sin^2(2\theta_{12}) + a^2 s_{13}^2 c_{23}^2 - a|r|s_{13}c_\delta \sin(2\theta_{12}) \sin(2\theta_{23})], \quad (5.15)$$

$$\begin{aligned} |(m_{\tilde{L}}^2)_{\tau \mu}|^2 \propto & \frac{|\Delta m_{31}^2|}{64v_T^2} \{ [4|r|s_{13}c_\delta \sin(2\theta_{12}) \cos(2\theta_{23}) + [2bc_{13}^2 - |r|(\cos(2\theta_{23}) - 3) \cos(2\theta_{12})] \\ & \times \sin(2\theta_{23}) ]^2 + 16r^2 c_\delta s_{13}^2 \sin(2\theta_{12}) \sin(2\theta_{23}) \}, \end{aligned} \quad (5.16)$$

where  $v_T$  and  $r$  have been defined in eqs. (4.3) and (4.17). The above expressions are valid for both the NO and IO neutrino mass spectrum with  $a$  and  $b$  defined as:

$$\text{NO : } a = 2(1 - |r|s_{12}^2) \simeq 2 \quad , \quad b = -2 + |r| \simeq -2, \quad (5.17)$$

$$\text{IO : } a = -2(1 + |r|s_{12}^2) \simeq -2 \quad , \quad b = 2 + |r| \simeq 2. \quad (5.18)$$

From the results shown in (5.14)–(5.16), one immediately concludes that the LFV elements of the soft breaking masses do not depend on the Majorana phases  $\alpha_{1,2}$  [28]. Moreover, the mass of the lightest neutrino ( $m_1$  or  $m_3$  depending on whether the neutrino mass spectrum is NO or IO) does not have any impact on the LFV terms  $(m_{\tilde{L}}^2)_{ij}$ , at the one-loop level [32, 33]. The independence of  $(m_\nu^\dagger m_\nu)_{ij}$  from the Majorana phases and absolute neutrino mass scale does not hold once we consider the two-loop RGEs for the soft masses. In this case, terms of the type

$$(m_{\tilde{L}}^2)_{ij} \propto \frac{m_0^2, A_0^2}{(16\pi^2)^2} [Y_T^\dagger (Y_e^\dagger Y_e)^T Y_T]_{ij} = \frac{m_0^2, A_0^2}{(16\pi^2)^2 v_T^2} \sum_{k=1}^3 y_{e_k}^2 [m_\nu^\dagger]_{ik} [m_\nu]_{kj}, \quad (5.19)$$

$$(m_{\tilde{L}}^2)_{ij} \propto \frac{m_0^2, A_0^2}{(16\pi^2)^2} \text{Tr}(Y_T^\dagger Y_T) [Y_T^\dagger Y_T]_{ij} = \frac{m_0^2, A_0^2}{(16\pi^2)^2 v_T^4} [m_\nu^\dagger m_\nu]_{ij} \sum_{k=1}^3 m_k^2, \quad (5.20)$$

$$(m_{\tilde{L}}^2)_{ij} \propto \frac{m_0^2, A_0^2}{(16\pi^2)^2} [Y_T^\dagger Y_T Y_T^\dagger Y_T]_{ij} = \frac{m_0^2, A_0^2}{(16\pi^2)^2 v_T^4} [m_\nu^\dagger m_\nu m_\nu^\dagger m_\nu]_{ij} \quad (5.21)$$

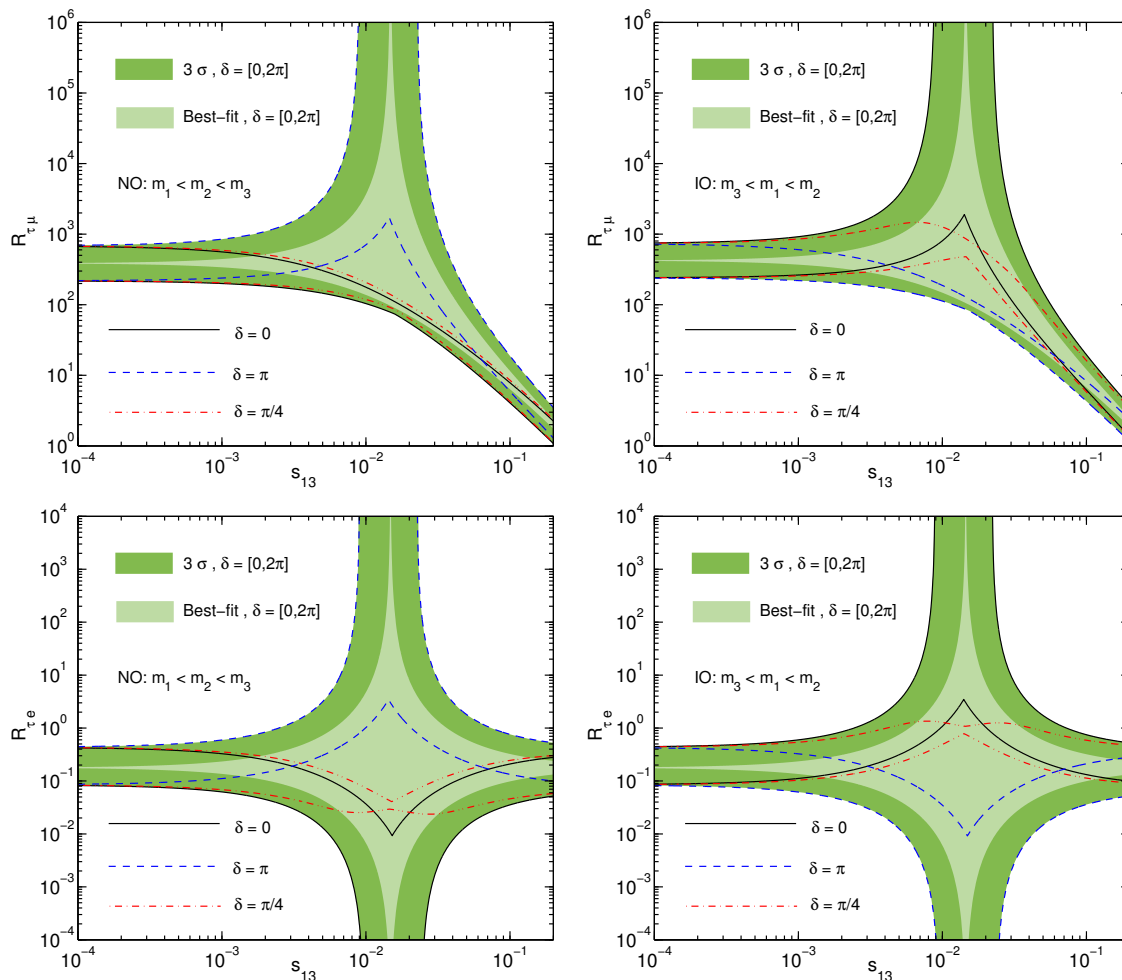


**Figure 3.** Allowed regions for  $R_{\tau\mu}$  (upper plots) and  $R_{\tau e}$  (lower plots) given in eqs. (5.10) and (5.13) as a function of  $s_{13}$  and  $\delta$ , for both the NO (left plots) and the IO (right plots) neutrino mass spectra. In dark green (light green) we show the  $3\sigma$  (best-fit) allowed regions obtained by varying the CP-violating phase  $\delta$  in the interval  $[0, 2\pi]$  and using the neutrino data displayed in table 3. The black solid (blue dashed) [red dash-dotted] line delimits the  $3\sigma$  region for  $\delta = 0$  ( $\delta = \pi$ ) [ $\delta = \pi/4$ ].

will be generated. The contributions of the form (5.19) do depend on  $\alpha_{1,2}$  and those of the form (5.20) and (5.21) depend on the mass of the lightest neutrino mass. However, being a two-loop effect, all those terms are negligible when compared with the one-loop ones. Hence, the quantities  $R_{\tau j}$  will be mainly sensitive to  $\theta_{13}$  and  $\delta$ .

The results for the ratios  $R_{\tau\mu}$  and  $R_{\tau e}$  obtained within the approximation described above and using the latest neutrino oscillation data summarised in table 3 are shown in figure 3 as functions of  $s_{13}$  for both NO (left plots) and IO (right plots) cases and for the entire possible range of  $\delta$  (see also ref. [55, 56]).

For  $s_{13} \rightarrow 0$ , the ratios  $R_{\tau\mu}$  and  $R_{\tau e}$  are given by (the quoted numbers are for the

best-fit values of  $\theta_{12}$ ,  $\theta_{23}$  and  $r$ , given in table 3)

$$R_{\tau\mu} = \frac{4(1 \mp |r|c_{12}^2)^2 s_{23}^2}{r^2 \sin^2(2\theta_{12})} \text{BR}(\tau \rightarrow \mu\nu_\tau\bar{\nu}_\mu) = 404.0_{-17.7}^{+18.1}(\text{IO}), \quad (5.22)$$

$$R_{\tau e} = \tan^2 \theta_{23} \text{BR}(\tau \rightarrow e\nu_\tau\bar{\nu}_e) = 0.18, \quad (5.23)$$

where the minus (plus) sign in the first equality of (5.22) corresponds to the case of a NO (IO) neutrino mass spectrum. Taking into account the uncertainties on the neutrino parameters reported in table 3, the following  $3\sigma$  ranges are obtained

$$R_{\tau\mu} = [260 (238), 696 (751)], R_{\tau e} = [0.8, 4.5] \times 10^{-1}, \quad (5.24)$$

where the numbers in parentheses correspond to the IO case.

The fact that  $R_{\tau\mu}$  is for  $s_{13} = 0$  larger than  $R_{\tau e}$  is due to the  $r^2$  suppression present in both  $|(m_{\bar{L}}^2)_{\mu e}|^2$  and  $|(m_{\bar{L}}^2)_{\tau e}|^2$ , but absent from  $|(m_{\bar{L}}^2)_{\tau\mu}|$  (see eqs. (5.14)–(5.16)). The above results also show that in the limit  $s_{13} \rightarrow 0$  the ratio  $R_{\tau\mu}$  is different for the NO and IO cases. This is due to the fact that, although  $|(m_{\bar{L}}^2)_{e\mu}|$  is the same in both scenarios, in the IO case  $|(m_{\bar{L}}^2)_{\tau\mu}|$  is slightly larger, as can be seen from eqs. (5.16) and (5.17).

The parameters  $\theta_{13}$  and  $\delta$  turn out to be crucial in determining the rates of the  $\mu e$  and  $\tau e$  LFV transitions. As  $\theta_{13}$  increases,  $|(m_{\bar{L}}^2)_{\mu e}|$  and  $|(m_{\bar{L}}^2)_{\tau e}|$  are either suppressed or enhanced, depending on the sign of  $\cos \delta$ . This can be seen from eqs. (5.14) and (5.15) where, for instance, cancelations among different terms are possible for specific values of  $\theta_{13}$ . The condition  $(m_{\bar{L}}^2)_{ij} \rightarrow 0$  automatically implies no Dirac-type CP violation in the neutrino sector: the Jarlskog CP invariant  $\mathcal{J}$  is proportional to  $\text{Im}[(m_{\nu}^\dagger m_\nu)_{12}(m_{\nu}^\dagger m_\nu)_{13}(m_{\nu}^\dagger m_\nu)_{23}]$  and since  $(m_{\nu}^\dagger m_\nu)_{ij} \propto (m_{\bar{L}}^2)_{ij}$ ,  $(m_{\bar{L}}^2)_{ij} \rightarrow 0$  implies  $\mathcal{J} \rightarrow 0$  [58]. However, by itself  $\mathcal{J} \rightarrow 0$  does not imply the absence of  $\mu - e$  and  $\tau - e$  transitions because the vanishing of  $(m_{\bar{L}}^2)_{\mu e}$  and  $(m_{\bar{L}}^2)_{\tau e}$  for  $\delta = 0$  require respectively:<sup>9</sup>

$$s_{13} = \mp \frac{1}{2} \frac{|r| \cot \theta_{23} \sin 2\theta_{12}}{1 \mp |r|s_{12}^2}, \quad s_{13} = \pm \frac{1}{2} \frac{|r| \tan \theta_{23} \sin 2\theta_{12}}{1 \mp |r|s_{12}^2}, \quad (5.25)$$

where the upper (lower) sign corresponds to the NO (IO) neutrino mass spectrum case. This shows clearly that simultaneous suppression of both  $\mu - e$  and  $\tau - e$  LFV transitions cannot occur: the sign of  $s_{13}$  in (5.25) required to suppress the former is always the opposite than that required to suppress the latter. Furthermore, inserting the best-fit values of table 3 in (5.25) one finds that the value of  $|s_{13}| \simeq 0.015$  for which one of these two transitions is suppressed is far beyond the sensitivity of future reactor neutrino experiments like Daya Bay [61], Double Chooz [62] or Reno [63]. Regarding the  $\tau\mu$  sector, we conclude that  $(m_{\bar{L}}^2)_{\tau\mu}$  shows a very weak dependence on  $\theta_{13}$  and  $\delta$  since the dominant term in eq. (5.16) is proportional to  $b^2 c_{13}^4 \sin^2(2\theta_{23}) \simeq 4$ , implying

$$|(m_{\bar{L}}^2)_{\tau\mu}| \simeq \frac{9m_0^2 + 3A_0^2}{16\pi^2} \frac{|\Delta m_{31}^2|}{v_T} \log \frac{\Lambda}{M_T}. \quad (5.26)$$

Moreover, the  $\tau - \mu$  transition cannot be suppressed because the limit  $|(m_{\bar{L}}^2)_{\tau\mu}| \rightarrow 0$  would require  $s_{13} \simeq 1$ , which is excluded by reactor neutrino experiments.

<sup>9</sup>The necessary conditions for the cancelation of  $(m_{\nu}^\dagger m_\nu)_{ij}$  have also been discussed in refs. [59, 60], albeit in a different context.

## 5.2 Large $\tan\beta$ effects on the ratios of branching ratios

In computing the ratios  $R_{\tau j}$  in section 5.1 several simplifications were made. Firstly, the running of  $m_\nu$  from  $m_Z$  to  $M_T$  was neglected. Secondly, the running of  $(m_L^2)_{ij}$  between  $M_G$  and  $M_T$  was treated in a simplified way and the running of  $(m_L^2)_{ij}$  (including its diagonal entries) between  $M_T$  and  $m_Z$  (or  $m_S$  - the SUSY scale) was neglected. Finally, the ratios  $R_{\tau j}$  were computed with the help of the simplified formula (5.11). In this section we will analyse scenarios in which some of these simplifications lead to incorrect results.

We first improve the approximate calculation of section 5.1 by taking into account the running of  $(m_L^2)_{ij}$  between  $M_G$  and  $M_T$  exactly. To this end we correct eq. (5.12) replacing it by

$$\left| \frac{(Y_T^\dagger Y_T)_{\tau j}}{(Y_T^\dagger Y_T)_{\mu e}} \right|_{\Lambda=M_T}^2 \simeq \left| \frac{(m_\nu^\dagger m_\nu)_{\tau j}}{(m_\nu^\dagger m_\nu)_{\mu e}} \right|_{\Lambda=M_T}^2, \quad (5.27)$$

with the right-hand side obtained by evolving  $m_\nu$  from  $m_Z$  to  $M_T$  with the help of the RGE (2.12). Alternatively, one can use eqs. (5.14)–(5.16) provided we take the values of all the neutrino parameters in these formulae at the scale  $\Lambda = M_T$ . We will illustrate the effects of this improvement by comparing the ratios  $|(m_L^2)_{\tau\mu}/(m_L^2)_{\mu e}|$  and  $|(m_L^2)_{\tau e}/(m_L^2)_{\mu e}|$  at the scale  $m_Z$  obtained using eqs. (5.12) and (5.27) with the ones resulting from the exact numerical computation of  $(m_L^2)_{ij}$  at the scale  $m_Z$ . The latter results are obtained as follows. We perform numerically the RG running of  $m_\nu$  from  $\Lambda = m_Z$  up to the  $M_T$  scale, extract the couplings  $Y_T$  and run them up to  $\Lambda = M_G$  using the TMSSM RGEs. At this scale, we impose universal boundary conditions on the SUSY-breaking terms and run all the couplings and masses down to low energies. We expect deviations between the approximation of section 5.1 and the improved and exact approaches to increase with  $\tan\beta$  because the running of the neutrino mass matrix is stronger for larger  $\tan\beta$  values.

In figure 4 we show  $|(m_L^2)_{\tau j}/(m_L^2)_{\mu e}|^2$  with  $j = e, \mu$  as a function of  $\tan\beta$  for the values of the input parameters  $m_0, m_{1/2}$  and  $A_0$  specified in the plots. We consider two benchmark values of  $s_{13}(m_Z)$ :  $s_{13} = 0$  (upper plots) and  $s_{13} = 0.2$  (lower plots). The results obtained by using the full numerical procedure are shown by the black-solid lines, while the red-dashed curves correspond to the approximations (5.27). The results extracted by means of the approximation of section 5.1 are shown by the black dash-dotted line which, of course, does not change with  $\tan\beta$ .

Let us first analyse the case  $s_{13}(m_Z) = 0$ . The deviations between the exact and the approximate results increase with increasing  $\tan\beta$  due to stronger RG effects. However, since we are considering the case of HI neutrino masses we would naively not expect such large effects even for large values of  $\tan\beta$  because the neutrino parameters run very little in this case. Although this is true for  $\theta_{12}, \theta_{23}$  and  $r$ , the same does not hold for  $\theta_{13}$ . Starting with a low-energy value  $\theta_{13}(m_Z)$ , we have at  $\Lambda = M_T$ :

$$\theta_{13}(M_T) \simeq \theta_{13}(m_Z) - \frac{y_\tau^2}{32\pi^2} \frac{r + \sqrt{r}}{1 - r} \sin(2\theta_{23}) \sin(2\theta_{12}) \ln\left(\frac{M_T}{m_Z}\right). \quad (5.28)$$

Taking  $\theta_{13}(m_Z) = 0$  and neglecting the RG effects on the parameters  $r, \theta_{12}$  and  $\theta_{23}$ , we



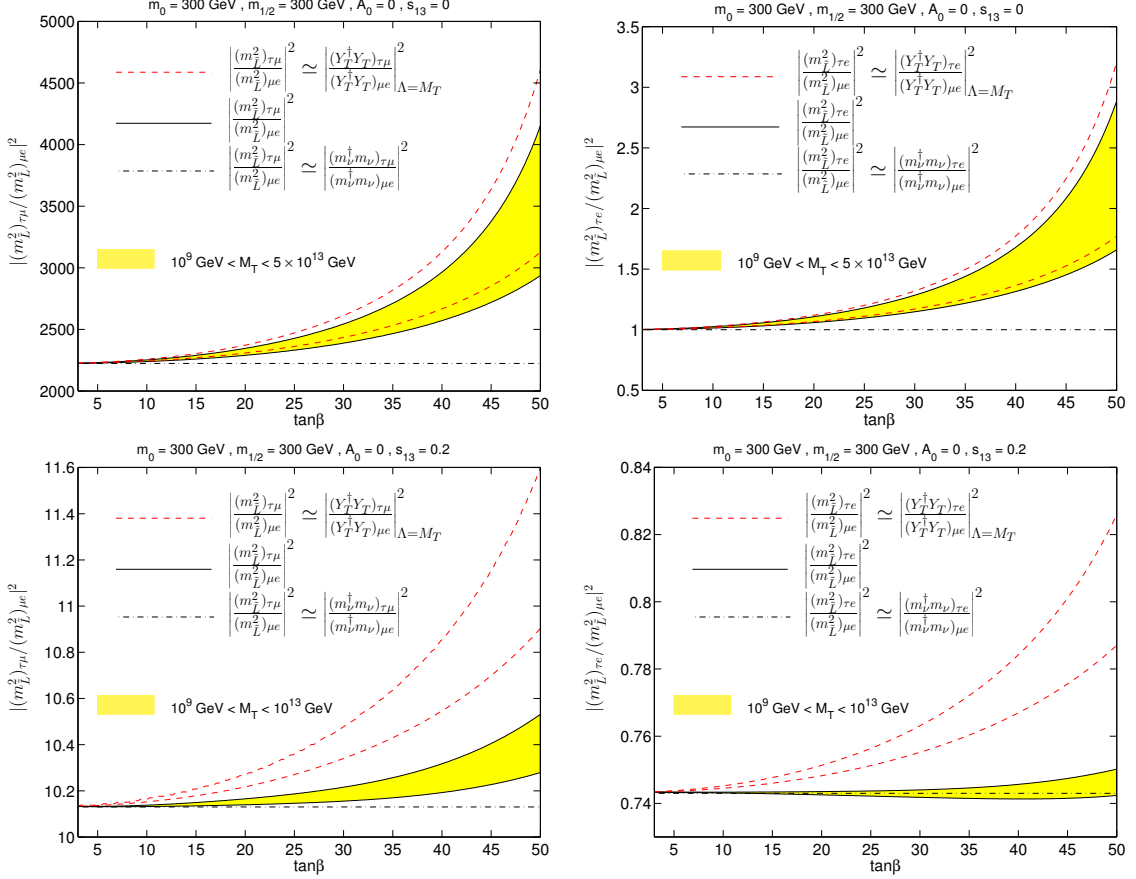


**Figure 4.** Ratios  $|(m_L^2)_{\tau\mu}/(m_L^2)_{\mu e}|^2$  (left plots) and  $|(m_L^2)_{\tau e}/(m_L^2)_{\mu e}|^2$  (right plots) as a function of  $\tan\beta$  for  $s_{13}(m_Z) = 0$  (upper plots) and  $s_{13}(m_Z) = 0.2$  (lower-plots). The black-solid lines correspond to the exact numerical result while the red-dashed ones were obtained using eq. (5.27) with  $Y_T$  taken at  $\Lambda = M_T$ . The horizontal dashed-dotted line indicates the value obtained using eq. (5.13) and the low-energy best-fit values for the neutrino parameters given in table 3 (all the CP-violating phases are set to zero). The red-dashed lines denote the values obtained using eq. (5.27) with  $Y_T$  taken at  $\Lambda = M_T$ . Filled in yellow are the regions (delimited by black-solid curves) (delimited by the black-solid curves) allowed for the  $M_T$  values indicated in each plot. The two red-dashed lines have been obtained for the two limiting values of such interval. All the plots have been obtained for  $m_0 = m_{1/2} = 300$  GeV,  $A_0 = 0$  and assuming a HI neutrino mass spectrum ( $m_1 = 0$  eV). For each value of  $M_T$  the value of  $\lambda_2$  has been chosen in such a way that for  $\tan\beta = 50$ ,  $\text{BR}(\mu \rightarrow e\gamma) \simeq 1.2 \times 10^{-11}$ .

obtain the following estimate for the value of  $\theta_{13}$  at the scale  $M_T$

$$\theta_{13}(M_T) \simeq -6.2 \times 10^{-8} \tan^2 \beta \ln \left( \frac{M_T}{m_Z} \right), \quad (5.29)$$

which reasonably agrees with the exact numerical result, even for large  $\tan\beta$ . Although small, these values of  $\theta_{13}$  at  $M_T$  may have some impact on the values of  $(Y_T^\dagger Y_T)_{ij}$  at that scale. Clearly, the effect will be stronger for larger values of  $\tan\beta$  and/or  $M_T$ . The fact that  $\theta_{13}(M_T)$  is negative leads to a suppression of  $|(Y_T^\dagger Y_T)_{\mu e}|$  with respect to the value



extracted using  $\theta_{13} = 0$ . This can be understood taking into account that the last term of eq. (5.14) becomes negative for  $\theta_{13} < 0$ . The opposite occurs for  $|(Y_T^\dagger Y_T)_{\tau e}|$  since the last contribution in eq. (5.15) is now positive, implying an enhancement of LFV in the  $\tau e$  sector. Since  $|(Y_T^\dagger Y_T)_{\tau \mu}|$  is practically insensitive to  $\theta_{13}$ , the RG effects on this quantity can be safely neglected. Therefore, we expect that the values of  $|(Y_T^\dagger Y_T)_{\tau \mu}/(Y_T^\dagger Y_T)_{\mu e}|^2$  and  $|(Y_T^\dagger Y_T)_{\tau e}/(Y_T^\dagger Y_T)_{\mu e}|^2$  at  $\Lambda = M_T$  are larger than the ones predicted for  $\theta_{13} = 0$ . This enhancement should be more significant in the latter case since  $|(Y_T^\dagger Y_T)_{\tau e}|$  grows and  $|(Y_T^\dagger Y_T)_{\mu e}|$  is suppressed. This is shown in figure 4 (upper plots) where one can see that the true values of  $|(m_L^2)_{\tau \mu}/(m_L^2)_{\mu e}|^2$  (left plot) and  $|(m_L^2)_{\tau e}/(m_L^2)_{\mu e}|^2$  (right plot) increase with  $\tan \beta$ . For  $\tan \beta = 50$ , the deviation of the exact result with respect to the one obtained in the crude approximation of section 5.1 (horizontal dashed-dotted lines) amounts to about 30% for  $M_T = 10^9$  GeV (lower black-solid line) and 90% for  $M_T = 10^{14}$  GeV (upper black-solid line) in the case of  $|(m_L^2)_{\tau \mu}/(m_L^2)_{\mu e}|^2$ . For  $|(m_L^2)_{\tau e}/(m_L^2)_{\mu e}|^2$ , one observes deviations of the order of 70% and 190%, for the same values of  $M_T$  and  $\tan \beta$ . Notice that the exact results (black-solid curves) are slightly lower than the ones obtained using eq. (5.27) (red-dashed curves). This deviation is due to the running of  $(m_L^2)_{ij}$  between  $M_T$  and  $m_Z$ . Considering the RGE of  $m_L^2$ , it can be shown that  $(m_L^2)_{ij}(m_Z)$  is approximately given by:

$$(m_L^2)_{ij}(m_Z) \simeq \left[ 1 - \frac{y_{e_i}^2 + y_{e_j}^2}{16\pi^2} \ln \left( \frac{M_T}{m_Z} \right) \right] (m_L^2)_{ij}(M_T), \quad (i \neq j = e, \mu, \tau), \quad (5.30)$$

where  $y_{e_i}$  are the charged-lepton Yukawa couplings. It is clear that this effect in  $(m_L^2)_{\mu e}$  can be neglected while for  $(m_L^2)_{\tau \mu, \tau e}$  one has:

$$(m_L^2)_{\tau \mu, \tau e}(m_Z) \simeq \left[ 1 - \frac{y_\tau^2}{16\pi^2} \ln \left( \frac{M_T}{m_Z} \right) \right] (m_L^2)_{\tau \mu, \tau e}(M_T). \quad (5.31)$$

Consequently, the ratios  $|(m_L^2)_{\tau j}/(m_L^2)_{\mu e}|^2$  obtained by solving the exact RGEs are enhanced with respect to those obtained in the improved approximation. Obviously, this effect is more relevant for large  $\tan \beta$ . Combining eqs. (5.30) and (5.31) we get the relation

$$\left| \frac{(m_L^2)_{\tau j}}{(m_L^2)_{\mu e}} \right|_{\Lambda=m_Z}^2 \simeq \left[ 1 - \frac{y_\tau^2}{8\pi^2} \ln \left( \frac{M_T}{m_Z} \right) \right] \left| \frac{(m_L^2)_{\tau j}}{(m_L^2)_{\mu e}} \right|_{\Lambda=M_T}^2, \quad (j = \mu, e), \quad (5.32)$$

which explains the deviation between the solid and dashed curves in figure 4.

When  $s_{13}(m_z) = 0.2$  (lower plots in figure 4), the running of the neutrino parameters does not affect much the quantities  $|(m_L^2)_{\tau j}/(m_L^2)_{\mu e}|^2$ . This stems from the fact that now the RG correction induced on  $\theta_{13}$  is negligible when compared with the low-energy value of this angle, as can be seen from eqs. (5.28) and (5.29). The deviations with respect to the approximate results are of the order of 10% (for the largest value of  $M_T$ ), as confirmed by comparing the red-dashed and dashed-dotted lines. Once more, the difference between the red-dashed and solid-black lines is due to the suppression factor shown in (5.32).

In figure 5 we confront the ratios  $R_{\tau \mu}$  and  $R_{\tau e}$  obtained (for the same set of parameters as in figure 4) by inserting into the simplified formula (5.11) exact values of

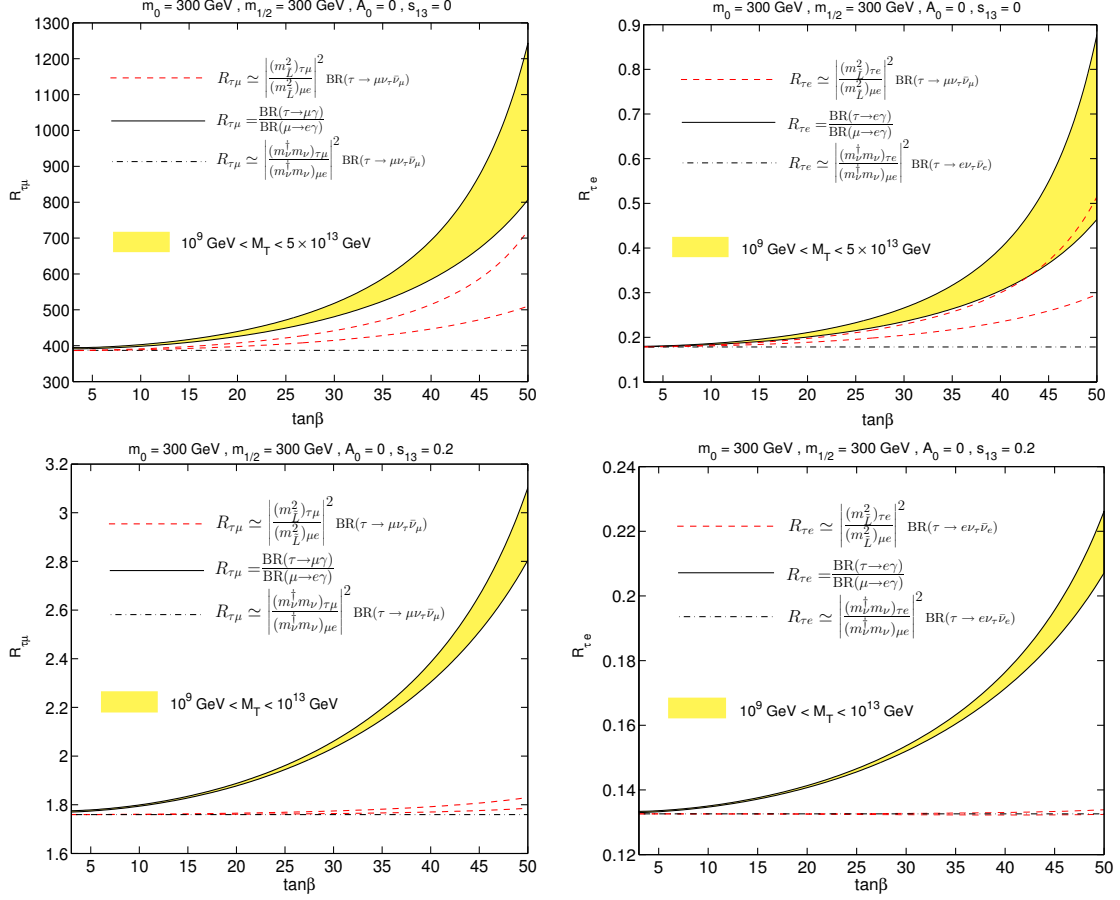


**Figure 5.** Ratios  $R_{\tau\mu}$  (left plots) and  $R_{\tau e}$  (right plots) as defined in eq. (5.11) for  $s_{13}(m_Z) = 0$  (upper plots) and  $s_{13}(m_Z) = 0.2$  (lower plots). The black-solid lines refer to the exact numerical result obtained performing the numerical RG running, full calculation of SUSY spectrum and exact computation of the one-loop  $\text{BR}(\ell_i \rightarrow \ell_j \gamma)$ . The red-dashed curves indicate the result obtained by means of eq. (5.11) using the exact values of  $|(m_L^2)_{ij}/(m_L^2)_{\mu e}|^2$ , while the dash-dotted horizontal line corresponds to the approximation of section 5.1.

$|(m_L^2)_{\tau j}/(m_L^2)_{\mu e}|^2$  obtained from the RG procedure with the ratios  $R_{\tau\mu}$  and  $R_{\tau e}$  obtained by the exact one-loop calculation of the individual branching fractions  $\text{BR}(\ell_i \rightarrow \ell_j \gamma)$  as e.g. in ref. [64]. Naively one would expect a good agreement between the red-dashed and solid-black curves since the former were obtained inserting the exact numerical results for the quantities  $|(m_L^2)_{ij}/(m_L^2)_{\mu e}|^2$  into eq. (5.10). However, this is not the case as can be observed in all plots in figure 5. The observed discrepancy is due to the fact that the formulae eqs. (5.8) and (5.9) with the same mass  $m_S$  can be a good approximation only if the slepton mass spectrum is not too much split: only then can the masses of the sleptons circulating in loop diagrams for the processes  $\ell_i \rightarrow \ell_j \gamma$  shown in figure 6 be replaced by an average mass  $m_S$ . In writing eq. (5.10) we have considered that  $m_S$  is the same for  $\tau \rightarrow \ell_j \gamma$  ( $\ell_j = e, \mu$ ) and  $\mu \rightarrow e \gamma$ . This is a valid approximation if the slepton masses are nearly degenerate for all three generations.

In the TMSSM with universal boundary conditions for the SUSY-breaking terms at

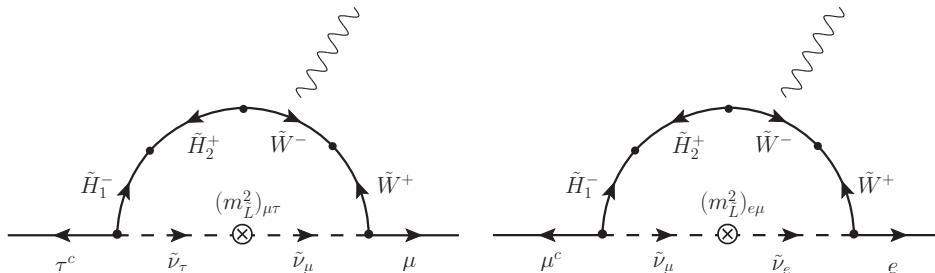


**Figure 6.** Example of one-loop (chargino-exchange) diagrams for the decays  $\tau \rightarrow \mu\gamma$  (left) and  $\mu \rightarrow e\gamma$  (right) in the mass insertion approximation. The crossed circles denote the corresponding LFV soft masses.

the GUT scale, the soft masses for the first two generations are approximately given by:

$$(m_{\tilde{f}}^2)_{ii}(m_Z) \simeq m_0^2 + \Delta M_{\tilde{f}}^2, \quad (5.33)$$

where  $\Delta M_{\tilde{f}}^2$  is the contribution due to the running of  $(m_{\tilde{f}}^2)_{ii}$  from the GUT scale down to low energies, which is mainly controlled by the terms  $g_a^2 |M_a|^2$  (where  $M_a$  is the  $G_a$  gaugino mass) present in the RGEs of the soft scalar masses. Performing the (one-loop) integration in the limit of vanishing Yukawa couplings, we obtain:

$$\Delta M_{\tilde{f}}^2 = 2 \sum_{a=1}^3 C_a^f m_{1/2}^2 \left\{ \frac{1}{b'_a} \left[ 1 - \frac{g_a^4(M_T)}{g_a^4(M_G)} \right] + \frac{1}{b_a} \frac{g_a^4(M_T)}{g_a^4(M_G)} \left[ 1 - \frac{g_a^4(m_Z)}{g_a^4(M_T)} \right] \right\}, \quad (5.34)$$

where  $C_a^f$  is the quadratic Casimir invariant of the representation of  $f$  under the gauge group  $G_a$ . The ratios of the gauge couplings appearing in the above equation are given by:

$$\frac{g_a^4(M_T)}{g_a^4(M_G)} = \left[ 1 - \frac{g_a^2(M_T)}{8\pi^2} b'_a \ln \left( \frac{M_G}{M_T} \right) \right]^2, \quad \frac{g_a^4(m_Z)}{g_a^4(M_T)} = \left[ 1 - \frac{g_a^2(m_Z)}{8\pi^2} b_a \ln \left( \frac{M_T}{m_Z} \right) \right]^2, \quad (5.35)$$

where  $b_a = (33/5, 1, -3)$  and  $b'_a = b_a + 7$  are the  $\beta$ -function coefficients in the RGEs of  $g_a$  for the MSSM and TMSSM cases, respectively [28]. The sneutrino masses of the first two generations (neglecting the D-term contributions and generation mixing) are given by  $m_{\tilde{\nu}_{e,\mu}}^2 \simeq m_0^2 + \Delta M_{\tilde{L}}^2$  with  $C_a^{\tilde{L}} = (3/20, 3/4, 0)$ . For large  $\tan \beta$ , the effects of the running due to the large  $\tau$  Yukawa coupling induce a nonnegligible splitting between the masses of  $\tilde{\nu}_\tau$  and  $\tilde{\nu}_{e,\mu}$ . In the limit of small  $Y_T$  couplings, one can show that

$$m_{\tilde{\nu}_\tau}^2 = m_{\tilde{\nu}_{e,\mu}}^2 - y_\tau^2 \frac{3m_0^2 + A_0^2}{8\pi^2} \ln \left( \frac{M_G}{m_Z} \right), \quad (5.36)$$

where, for simplicity, we have approximated  $y_\tau$  between  $M_G$  and  $m_Z$  by a constant. The term proportional to  $y_\tau^2$  is always negative making the  $\tau$ -sneutrino lighter than the remaining two. In order to account for the effect of the sneutrino mass splitting on the quantities  $R_{\tau j}$ , we correct eq. (5.11) with a factor  $\eta$

$$R_{\tau j} \simeq \eta \left| \frac{(m_{\tilde{L}}^2)_{\tau j}}{(m_{\tilde{L}}^2)_{\mu e}} \right|^2 \text{BR}(\tau \rightarrow \ell_j \nu_\tau \bar{\nu}_j), \quad \eta = \left[ \frac{F(m_{\tilde{\nu}_\tau}^2, m_{\tilde{\nu}_j}^2, m_S^i)}{F(m_{\tilde{\nu}_\mu}^2, m_{\tilde{\nu}_e}^2, m_S^i)} \right]^2, \quad (5.37)$$

where  $F$  denotes the loop function of the corresponding decay amplitude and  $m_S^i$  the masses of the non-sleptonic particles running inside the loops.

Deviations<sup>10</sup> from the limit  $\eta = 1$  are expected to grow with increasing  $\tan\beta$  because the mass splitting between  $\tilde{\nu}_{e,\mu}$  and  $\tilde{\nu}_\tau$  increases<sup>11</sup> with  $\tan\beta$ . This can be observed in figure 5. The differences between the exact numerical results for  $R_{\tau j}$  (black-solid curves) and the ones obtained by using eq. (5.10) together with the real values of the LFV soft masses (red-dashed lines) increase with  $\tan\beta$ . Moreover,  $\eta$  depends on the initial values of  $m_0$ ,  $m_{1/2}$  and  $A_0$  which for large  $\tan\beta$  leads to a variation of  $R_{\tau\mu}$  and  $R_{\tau e}$  in the SUSY parameter space, even for fixed values of  $M_T$ ,  $\lambda_2$  and the neutrino parameters. Finally, it is worth stressing that this effect does not depend on the way through which LFV in the soft masses is generated. Hence, it should also be present in the SUSY version of the type-I seesaw.

In order to study the behaviour of  $R_{\tau j}$  in the SUSY  $(m_{1/2}, m_0)$  parameter space, we present two examples in figures 7 and 8 for  $\tan\beta = 10$  and 50, respectively. Both figures show the variation of  $R_{\tau\mu}$  (left plots) and  $R_{\tau e}$  (right plots) for  $s_{13}(m_Z) = 0$  (upper plots) and  $s_{13}(m_Z) = 0.2$  (lower plots). The blue-solid lines indicate the contours corresponding to  $\text{BR}(\mu \rightarrow e\gamma) = 10^{-12}, 10^{-13}$  and the hatched regions are excluded by the MEGA bound  $\text{BR}(\mu \rightarrow e\gamma) < 1.2 \times 10^{-11}$  [51]. In cyan and light grey we show the regions where the mass of the lightest slepton  $m_{\tilde{\ell}_1}$  is below 100 GeV (the dashed-dotted line corresponds to  $m_{\tilde{\ell}_1} = 200$  GeV) and the lightest supersymmetric particle (LSP) is charged, respectively. To the left of the black-dashed line the lightest chargino mass violates the LEP bound  $m_{\chi_1^\pm} > 104$  GeV [65].

Figure 7 shows that for  $\tan\beta = 10$  (moderate RG running of the neutrino sector parameters and slepton mass splitting) the ratios  $R_{\tau\mu}$  and  $R_{\tau e}$  vary in the range of 10% at most, in the whole SUSY parameter space. Moreover, the approximate estimates of these ratios given by eqs. (5.22) and (5.23) are in good agreement with the exact results. In contrast, for  $\tan\beta = 50$  (figure 8) we see that the ratios of BRs  $R_{\tau j}$  are considerably enhanced for  $s_{13}(m_Z) = 0$  due to the RG effects on  $\theta_{13}$ , as previously discussed. Also, the variation of  $R_{\tau\mu}$  and  $R_{\tau e}$  in the SUSY parameter space is now more pronounced due to the larger mass-splitting induced in the slepton masses (see discussion above). The observed enhancement with respect to the case in which all sleptons are degenerate is due to the factor  $\eta$  defined in eq. (5.37) which depends on  $m_{1/2}$  and  $m_0$ , as seen in figure 8.

## 6 Summary and concluding remarks

It is well known that RG effects may induce important corrections to neutrino masses and mixing. This subject has been extensively studied in the literature in the effective-theory framework and also in the context of the type I seesaw mechanism. In this work we have addressed this problem in a supersymmetric scenario where heavy triplet states are added

<sup>10</sup>These deviations are negligible for the ratio  $\text{BR}(\tau \rightarrow \mu\gamma)/\text{BR}(\tau \rightarrow e\gamma)$  since  $\eta \simeq 1$ , irrespective of the value  $\tan\beta$ .

<sup>11</sup>One should recall that the dependence of  $\eta$  on the initial conditions at  $M_G$  is non-trivial. Although we will not address the analytical treatment of this subject here, we will show some numerical examples in the following. The loop functions for the various LFV operators in the two-generation limit can be found in ref. [66]

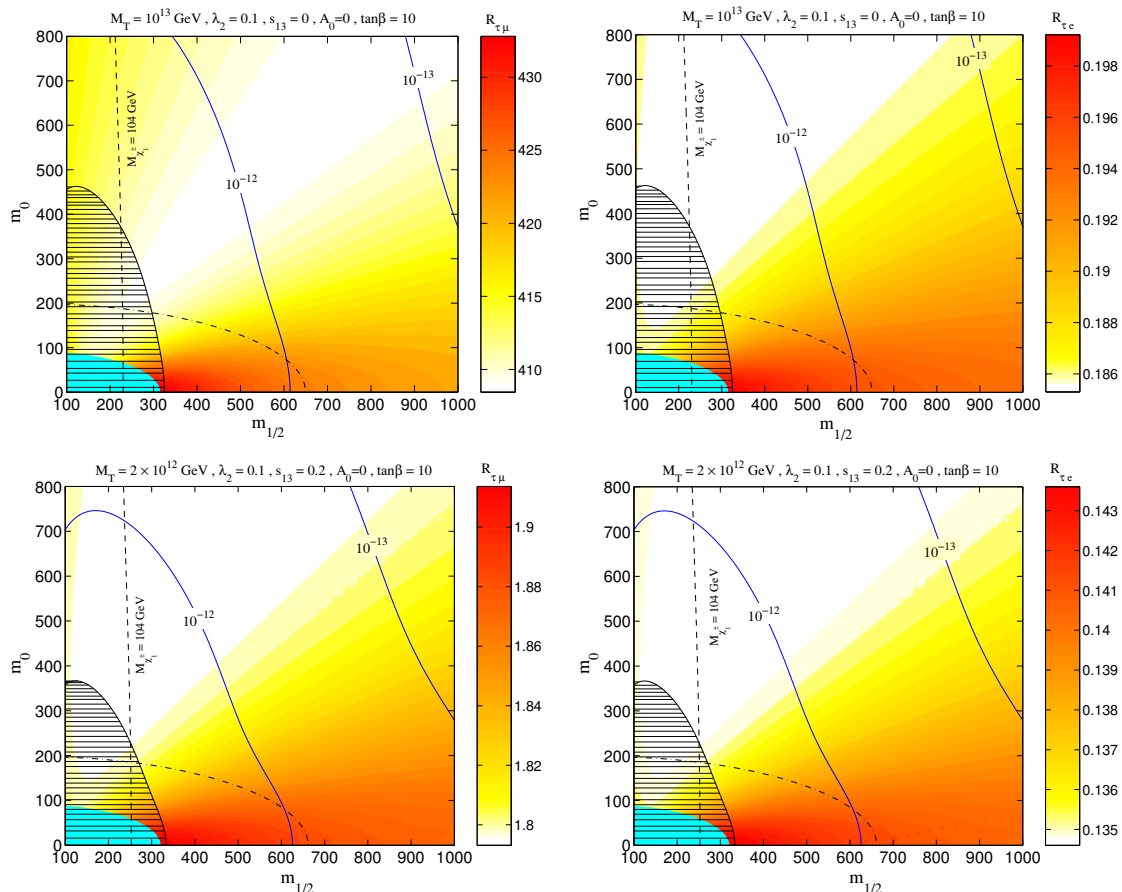


**Figure 7.** Variation of  $R_{\tau\mu}$  (left plots) and  $R_{\tau e}$  (right plots) in the  $(m_{1/2}, m_0)$  parameter space for  $s_{13}(m_Z) = 0$  (upper plots) and 0.2 (lower plots) and  $\tan\beta = 10$  (the values of  $M_T$ ,  $\lambda_2$  and  $A_0$  are indicated on the top of each plot and the remaining low-energy parameters are taken at their best-fit points). The mass of the lightest slepton  $m_{\tilde{\ell}_1}$  is below 100 GeV inside the regions filled in cyan and the black dashed-dotted line corresponds to  $m_{\tilde{\ell}_1} = 200$  GeV. To the left of the black-dashed line the lightest-chargino mass is below the LEP bound. The black-hatched region is excluded by the MEGA bound  $\text{BR}(\mu \rightarrow e\gamma) < 1.2 \times 10^{-11}$  [51] and the blue contours correspond to  $\text{BR}(\mu \rightarrow e\gamma) = 10^{-12}, 10^{-13}$ . The variation of  $R_{\tau j}$  follows the colour bars shown on the right of each panel.

to the MSSM field content. We started by obtaining the RGE for the effective neutrino mass operator in an SU(5) model in which the triplet superfields can be accommodated in a 15-dimensional representation. The general expressions for the RGEs of the neutrino mixing angles, masses and CP-violating phases were also derived. Taking the pure type II seesaw case, we have analysed both analytically and numerically the effect of the couplings  $Y_T$  on the RG flow of the neutrino masses and mixing. Our results can be summarised as follows:

- We have pointed out some differences between the present results and those previously obtained in ref. [27]. Apart from discrepancies in the RGEs, we have shown that for energies above  $M_T$  the RG flow of the neutrino mixing angles and CP phases does depend on the Majorana phases.

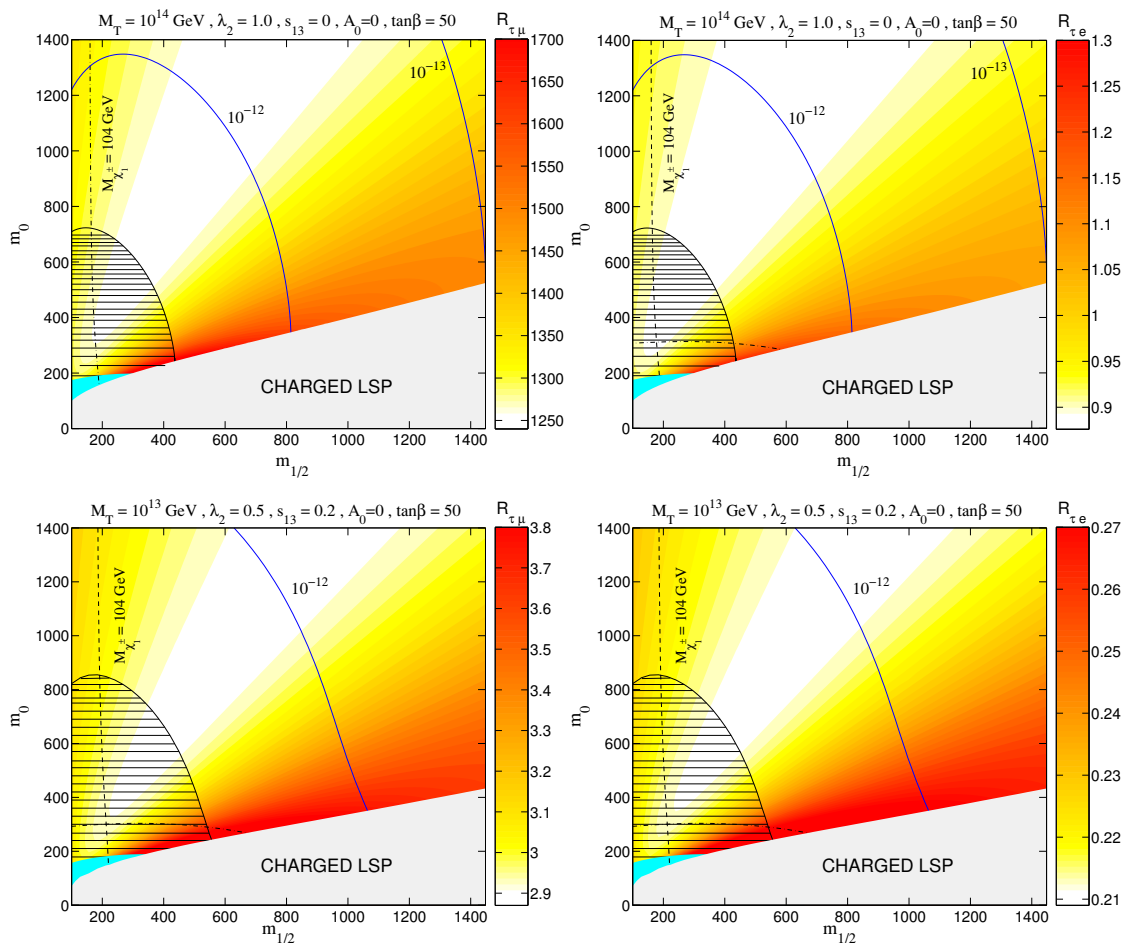


**Figure 8.** The same as in figure 7 for  $\tan\beta = 50$ . Inside the light-grey regions the LSP is charged.

- The RG-induced effects on the neutrino masses and mixing angles due to the presence of the heavy triplet states become more relevant as the size of the couplings  $Y_T$  increases. These new effects are not sensitive to the value of  $\tan\beta$  and may be equally relevant in a non-SUSY case. The running contributions controlled by  $Y_T$  are more important for the parameter  $r$  (the ratio between the solar and atmospheric neutrino mass squared differences) and the atmospheric neutrino mixing angle. Regarding the running of the CP-violating phases  $\delta$  and  $\alpha_{1,2}$ , we have shown that the RG effects induced by the couplings  $Y_T$  are negligible.
- Within the bottom-up approach, we have worked out some numerical examples (for both HI and IH neutrino mass spectra) with the purpose of quantifying the running effects on  $r$  and  $\theta_{23}$ . We have shown that if  $y_i \sim \mathcal{O}(1)$ , then the values of  $\theta_{23}$  and  $r$  at the GUT scale are outside their present low-energy  $3\sigma$  intervals. This means that type II seesaw-based models for neutrino masses and mixing with large  $Y_T$  couplings should not predict neutrino mass and mixing parameters at a high scale in agreement with the low-energy data and, therefore, a consistent RG analysis is demanded.



The second part of this work has been devoted to the analysis of the LFV charged-lepton radiative decays  $\ell_i \rightarrow \ell_j \gamma$  and their connection to low-energy neutrino data in the framework of the TMSSM with universal boundary conditions for the soft SUSY-breaking terms. After having updated the approximate predictions for the ratios of BRs  $R_{\tau j} = \text{BR}(\ell_i \rightarrow \ell_j \gamma) / \text{BR}(\mu \rightarrow e \gamma)$ , we compared them with the exact numerical results. The predictions depend on the value of  $\tan \beta$  and, of course, on the value of the yet unknown neutrino parameters  $\theta_{13}$  and  $\delta$ . To summarise the results of this part, let us review the two extreme limits of low and high  $\tan \beta$ .

- **Small  $\tan \beta$**

If  $\tan \beta$  is small, the RG-induced effects on the neutrino mass and mixing parameters can be safely neglected, and the ratios of branching ratios  $R_{\tau j}$  ( $j = e, \mu$ ) only depend on two parameters:  $\delta$  and  $\theta_{13}$ . Furthermore, the approximate results are in good agreement with the exact numerical ones. For  $\theta_{13} = 0$ , we have shown that the  $3\sigma$  allowed interval for  $R_{\tau \mu}$  is  $R_{\tau \mu} = [260 (238), 696 (751)]$  (where the numbers in parentheses refer to the IO neutrino mass spectrum case). This means that, if  $\text{BR}(\mu \rightarrow e \gamma) \sim 10^{-11}$  (close to the present upper bound), then  $\tau \rightarrow \mu \gamma$  could be observed with a future sensitivity of  $10^{-9}$ , reachable at the SuperKEKB [67] upgrade and SUPERB [68] flavour factories. However, if the bound on  $\text{BR}(\mu \rightarrow e \gamma)$  is lowered to  $10^{-12}$ , then an observation of  $\tau \rightarrow \mu \gamma$  at the level of  $10^{-9}$  or above would be in conflict with the predictions of the model for small  $\tan \beta$  and  $\theta_{13} = 0$ . For the  $\tau \rightarrow e \gamma$  decay, its BR is too small to allow for its future observation.

Considering now values of  $\theta_{13}$  close to the experimentally allowed upper bound ( $\theta_{13} \simeq 0.2$ ), the predictions for  $R_{\tau \mu}$  show that an observation of  $\tau \rightarrow \mu \gamma$  above  $10^{-9}$  would exclude the TMSSM with universal boundary conditions for the SUSY breaking terms at the GUT scale. This stems from the fact that for  $\theta_{13} \gtrsim 0.1$  (and considering  $\text{BR}(\mu \rightarrow e \gamma) < 10^{-11}$ ),  $\text{BR}(\tau \rightarrow \mu \gamma) \lesssim 10^{-10}$ . For the  $\tau \rightarrow e \gamma$  decay, its observation with  $\text{BR}(\tau \rightarrow e \gamma) \gtrsim 10^{-9}$  would also be in conflict with the TMSSM if  $\theta_{13}$  is close to its upper bound. Nevertheless, for  $\theta_{13} \sim 0.015$  flavour suppressions in the  $\mu e$  and  $\tau e$  slepton masses may occur and, under special conditions, all the three LFV decays could be observed.

- **Large  $\tan \beta$**

We have concluded that if  $\tan \beta$  is large the values of  $R_{\tau j}$  may deviate considerably from the approximate ones. Moreover, in this  $\tan \beta$  regime the splitting between the third generation slepton masses and the remaining two introduces a non-trivial dependence of  $R_{\tau j}$  on the soft SUSY-breaking masses. This is in contrast with the low  $\tan \beta$  limit in which the slepton mass splitting is much less pronounced. We have shown that the running of the unknown mixing angle  $\theta_{13}$  from the electroweak to the heavy-triplet decoupling scale may affect the relative magnitude of various LFV soft slepton masses, especially in the case of a very small  $\theta_{13}$ . In short, this means that ignoring the RG running in estimating the rates of the LFV processes on the basis of the neutrino data may lead to misleading predictions for the rates of the LFV

decays. Therefore, for large  $\tan\beta$ , the only way to obtain reliable results is to perform a complete numerical calculation. In particular,  $R_{\tau\mu}$  may be enhanced by a factor of four (or even larger) when going from  $\tan\beta = 10$  to  $\tan\beta = 50$ , for the same set of initial conditions (see figures 7 and 8). Consequently, if  $\tan\beta$  is large (and  $\theta_{13}$  is close to zero)  $\text{BR}(\tau \rightarrow \mu\gamma)$  can reach the value of  $10^{-9}$  (and, therefore, be experimentally detectable) even if  $\text{BR}(\mu \rightarrow e\gamma)$  is as low as  $10^{-12}$ . Still, the simultaneous observation of  $\mu \rightarrow e\gamma$  and any of the two radiative  $\tau$  decays would strongly disfavour the present scenario for large  $\theta_{13}$ , even in the high  $\tan\beta$  regime.

In conclusion, we have shown that the RG corrections in the framework of the TMSSM may be important when making predictions regarding neutrino masses and mixings. These radiative effects become more relevant when the couplings between the lepton doublets and the heavy triplet are large. On the other hand, provided that  $\tan\beta$  is large, important effects may be observed on the LFV decay rates even if the couplings  $Y_T$  are small. In such a situation, the knowledge of all low-energy neutrino parameters and SUSY mass spectrum is crucial for an accurate prediction of the LFV decay rates. Nevertheless, the approximate results for the ratios of BRs in distinct channels are reliable if  $\tan\beta$  is not too large.

## Acknowledgments

We are grateful to M. Maltoni and C. Savoy for discussions and to A. Rossi and A. M. Teixeira for the careful reading of the manuscript and the numerous comments and suggestions. The author also thanks M. A. Schmidt for several private communications regarding the results obtained in ref. [27].

**Open Access.** This article is distributed under the terms of the Creative Commons Attribution Noncommercial License which permits any noncommercial use, distribution, and reproduction in any medium, provided the original author(s) and source are credited.

## References

- [1] P. Minkowski,  $\mu \rightarrow e\gamma$  at a Rate of One Out of 1-Billion Muon Decays?, *Phys. Lett.* **B 67** (1977) 421 [SPIRES].
- [2] M. Gell-Mann, P. Ramond and R. Slansky, *Complex spinors and unified theories*, in *Supergravity*, eds. P. Van Nieuwenhuizen and D. Freedman, North-Holland, Amsterdam The Neatherland (1979), pg. 315.
- [3] T. Yanagida, *Horizontal gauge symmetry and masses of neutrinos*, in *Proceedings of the Baryon Number of the Universe and Unified Theoris*, eds. O. Sawada and A. Sugamoto KEK, Tsukuba (1979), pg. 95.
- [4] S.L. Glashow, *The future of elementary particle physics*, *NATO Adv. Study Inst. Ser. B Phys.* **59** (1979) 687.
- [5] R.N. Mohapatra and G. Senjanović, *Neutrino mass and spontaneous parity nonconservation*, *Phys. Rev. Lett.* **44** (1980) 912 [SPIRES].



- [6] G. Altarelli and F. Feruglio, *Theoretical models of neutrino masses and mixings*, *Springer Tracts Mod. Phys.* **190** (2003) 169 [[hep-ph/0206077](#)] [[SPIRES](#)].
- [7] G. Altarelli and F. Feruglio, *Models of neutrino masses and mixings*, *New J. Phys.* **6** (2004) 106 [[hep-ph/0405048](#)] [[SPIRES](#)].
- [8] R.N. Mohapatra and A.Y. Smirnov, *Neutrino Mass and New Physics*, *Ann. Rev. Nucl. Part. Sci.* **56** (2006) 569 [[hep-ph/0603118](#)] [[SPIRES](#)].
- [9] M.C. Gonzalez-Garcia and M. Maltoni, *Phenomenology with Massive Neutrinos*, *Phys. Rept.* **460** (2008) 1 [[arXiv:0704.1800](#)] [[SPIRES](#)].
- [10] T. Schwetz, M.A. Tortola and J.W.F. Valle, *Three-flavour neutrino oscillation update*, *New J. Phys.* **10** (2008) 113011 [[arXiv:0808.2016](#)] [[SPIRES](#)].
- [11] P.H. Chankowski and S. Pokorski, *Quantum corrections to neutrino masses and mixing angles*, *Int. J. Mod. Phys. A* **17** (2002) 575 [[hep-ph/0110249](#)] [[SPIRES](#)].
- [12] K.R.S. Balaji, A.S. Dighe, R.N. Mohapatra and M.K. Parida, *Radiative magnification of neutrino mixings and a natural explanation of the neutrino anomalies*, *Phys. Lett. B* **481** (2000) 33 [[hep-ph/0002177](#)] [[SPIRES](#)].
- [13] R.N. Mohapatra, M.K. Parida and G. Rajasekaran, *High scale mixing unification and large neutrino mixing angles*, *Phys. Rev. D* **69** (2004) 053007 [[hep-ph/0301234](#)] [[SPIRES](#)].
- [14] S. Antusch, J. Kersten, M. Lindner and M. Ratz, *The LMA solution from bimaximal lepton mixing at the GUT scale by renormalization group running*, *Phys. Lett. B* **544** (2002) 1 [[hep-ph/0206078](#)] [[SPIRES](#)].
- [15] T. Miura, T. Shindou and E. Takasugi, *The renormalization group effect to the bi-maximal mixing*, *Phys. Rev. D* **68** (2003) 093009 [[hep-ph/0308109](#)] [[SPIRES](#)].
- [16] Y. Farzan and M.E. Peskin, *The contribution from neutrino Yukawa couplings to lepton electric dipole moments*, *Phys. Rev. D* **70** (2004) 095001 [[hep-ph/0405214](#)] [[SPIRES](#)].
- [17] S. Antusch, J. Kersten, M. Lindner, M. Ratz and M.A. Schmidt, *Running neutrino mass parameters in see-saw scenarios*, *JHEP* **03** (2005) 024 [[hep-ph/0501272](#)] [[SPIRES](#)].
- [18] J.-w. Mei, *Running neutrino masses, leptonic mixing angles and CP-violating phases: From  $M(Z)$  to  $\Lambda(GUT)$* , *Phys. Rev. D* **71** (2005) 073012 [[hep-ph/0502015](#)] [[SPIRES](#)].
- [19] R. Barbieri, D.V. Nanopoulos, G. Morchio and F. Strocchi, *Neutrino Masses in Grand Unified Theories*, *Phys. Lett. B* **90** (1980) 91 [[SPIRES](#)].
- [20] T.P. Cheng and L.-F. Li, *Neutrino Masses, Mixings and Oscillations in  $SU(2) \times U(1)$  Models of Electroweak Interactions*, *Phys. Rev. D* **22** (1980) 2860 [[SPIRES](#)].
- [21] M. Magg and C. Wetterich, *Neutrino mass problem and gauge hierarchy*, *Phys. Lett. B* **94** (1980) 61 [[SPIRES](#)].
- [22] J. Schechter and J.W.F. Valle, *Neutrino Masses in  $SU(2) \times U(1)$  Theories*, *Phys. Rev. D* **22** (1980) 2227 [[SPIRES](#)].
- [23] R.N. Mohapatra and G. Senjanović, *Neutrino Masses and Mixings in Gauge Models with Spontaneous Parity Violation*, *Phys. Rev. D* **23** (1981) 165 [[SPIRES](#)].
- [24] G. Lazarides, Q. Shafi and C. Wetterich, *Proton Lifetime and Fermion Masses in an  $SO(10)$  Model*, *Nucl. Phys. B* **181** (1981) 287 [[SPIRES](#)].

- [25] E. Ma and U. Sarkar, *Neutrino masses and leptogenesis with heavy Higgs triplets*, *Phys. Rev. Lett.* **80** (1998) 5716 [[hep-ph/9802445](#)] [[SPIRES](#)].
- [26] W. Chao and H. Zhang, *One-loop renormalization group equations of the neutrino mass matrix in the triplet seesaw model*, *Phys. Rev. D* **75** (2007) 033003 [[hep-ph/0611323](#)] [[SPIRES](#)].
- [27] M.A. Schmidt, *Renormalization Group Evolution in the type-I + II seesaw model*, *Phys. Rev. D* **76** (2007) 073010 [[arXiv:0705.3841](#)] [[SPIRES](#)].
- [28] A. Rossi, *Supersymmetric seesaw without singlet neutrinos: Neutrino masses and lepton-flavour violation*, *Phys. Rev. D* **66** (2002) 075003 [[hep-ph/0207006](#)] [[SPIRES](#)].
- [29] F. Borzumati and T. Yamashita, *Minimal supersymmetric SU(5) model with nonrenormalizable operators: Seesaw mechanism and violation of flavour and CP*, [arXiv:0903.2793](#) [[SPIRES](#)].
- [30] F. Borzumati and A. Masiero, *Large Muon and electron Number Violations in Supergravity Theories*, *Phys. Rev. Lett.* **57** (1986) 961 [[SPIRES](#)].
- [31] M. Raidal et al., *Flavour physics of leptons and dipole moments*, *Eur. Phys. J. C* **57** (2008) 13 [[arXiv:0801.1826](#)] [[SPIRES](#)].
- [32] F.R. Joaquim and A. Rossi, *Gauge and Yukawa mediated supersymmetry breaking in the triplet seesaw scenario*, *Phys. Rev. Lett.* **97** (2006) 181801 [[hep-ph/0604083](#)] [[SPIRES](#)].
- [33] F.R. Joaquim and A. Rossi, *Phenomenology of the triplet seesaw mechanism with Gauge and Yukawa mediation of SUSY breaking*, *Nucl. Phys. B* **765** (2007) 71 [[hep-ph/0607298](#)] [[SPIRES](#)].
- [34] M. Hirsch, S. Kaneko and W. Porod, *Supersymmetric seesaw type-II: LHC and lepton flavour violating phenomenology*, *Phys. Rev. D* **78** (2008) 093004 [[arXiv:0806.3361](#)] [[SPIRES](#)].
- [35] J.N. Esteves et al., *Flavour violation at the LHC: type-I versus type-II seesaw in minimal supergravity*, *JHEP* **05** (2009) 003 [[arXiv:0903.1408](#)] [[SPIRES](#)].
- [36] L. Calibbi, M. Frigerio, S. Lavignac and A. Romanino, *Flavour violation in supersymmetric SO(10) unification with a type-II seesaw mechanism*, *JHEP* **12** (2009) 057 [[arXiv:0910.0377](#)] [[SPIRES](#)].
- [37] S. Weinberg, *Non-renormalization theorems in non-renormalizable theories*, *Phys. Rev. Lett.* **80** (1998) 3702 [[hep-th/9803099](#)] [[SPIRES](#)].
- [38] R. Barbieri, S. Ferrara, L. Maiani, F. Palumbo and C.A. Savoy, *Quartic mass matrix and renormalization constants in supersymmetric Yang-Mills theories*, *Phys. Lett. B* **115** (1982) 212 [[SPIRES](#)].
- [39] N.K. Falck, *Renormalization Group Equations for Softly Broken Supersymmetry: The Most General Case*, *Z. Phys. C* **30** (1986) 247 [[SPIRES](#)].
- [40] S.P. Martin and M.T. Vaughn, *Two loop renormalization group equations for soft supersymmetry breaking couplings*, *Phys. Rev. D* **50** (1994) 2282 [Erratum *ibid.* **D 78** (2008) 039903] [[hep-ph/9311340](#)] [[SPIRES](#)].
- [41] S. Weinberg, *Baryon and Lepton Nonconserving Processes*, *Phys. Rev. Lett.* **43** (1979) 1566 [[SPIRES](#)].
- [42] J.A. Casas, J.R. Espinosa and I. Navarro, *New supersymmetric source of neutrino masses and mixings*, *Phys. Rev. Lett.* **89** (2002) 161801 [[hep-ph/0206276](#)] [[SPIRES](#)].

- [43] J.A. Casas, J.R. Espinosa and I. Navarro, *Large mixing angles for neutrinos from infrared fixed points*, *JHEP* **09** (2003) 048 [[hep-ph/0306243](#)] [[SPIRES](#)].
- [44] P.H. Chankowski and Z. Pluciennik, *Renormalization group equations for seesaw neutrino masses*, *Phys. Lett. B* **316** (1993) 312 [[hep-ph/9306333](#)] [[SPIRES](#)].
- [45] K.S. Babu, C.N. Leung and J.T. Pantaleone, *Renormalization of the neutrino mass operator*, *Phys. Lett. B* **319** (1993) 191 [[hep-ph/9309223](#)] [[SPIRES](#)].
- [46] S. Antusch, M. Drees, J. Kersten, M. Lindner and M. Ratz, *Neutrino mass operator renormalization in two Higgs doublet models and the MSSM*, *Phys. Lett. B* **525** (2002) 130 [[hep-ph/0110366](#)] [[SPIRES](#)].
- [47] K.S. Babu, *Renormalization group analysis of the Kobayashi-Maskawa matrix*, *Z. Phys. C* **35** (1987) 69 [[SPIRES](#)].
- [48] P.H. Chankowski, W. Krolikowski and S. Pokorski, *Fixed points in the evolution of neutrino mixings*, *Phys. Lett. B* **473** (2000) 109 [[hep-ph/9910231](#)] [[SPIRES](#)].
- [49] J.A. Casas, J.R. Espinosa, A. Ibarra and I. Navarro, *General RG equations for physical neutrino parameters and their phenomenological implications*, *Nucl. Phys. B* **573** (2000) 652 [[hep-ph/9910420](#)] [[SPIRES](#)].
- [50] S. Antusch, J. Kersten, M. Lindner and M. Ratz, *Running neutrino masses, mixings and CP phases: Analytical results and phenomenological consequences*, *Nucl. Phys. B* **674** (2003) 401 [[hep-ph/0305273](#)] [[SPIRES](#)].
- [51] MEGA collaboration, M.L. Brooks et al., *New Limit for the Family-Number Non-conserving Decay  $\mu^+ \rightarrow e\gamma$* , *Phys. Rev. Lett.* **83** (1999) 1521 [[hep-ex/9905013](#)] [[SPIRES](#)].
- [52] BABAR collaboration, B. Aubert et al., *Search for lepton flavor violation in the decay  $\tau^\pm \rightarrow e^\pm\gamma$* , *Phys. Rev. Lett.* **96** (2006) 041801 [[hep-ex/0508012](#)] [[SPIRES](#)].
- [53] BELLE collaboration, K. Hayasaka et al., *New search for  $\tau \rightarrow \mu\gamma$  and  $\tau \rightarrow e\gamma$  decays at Belle*, *Phys. Lett. B* **666** (2008) 16 [[arXiv:0705.0650](#)] [[SPIRES](#)].
- [54] S. Banerjee, *Searches for lepton flavor violating decays  $\tau^\pm \rightarrow \ell^\pm\gamma$ ,  $\tau^\pm \rightarrow \ell^\pm P0$  (where  $\ell^- = e^-, \mu^-$  and  $P0 = \pi^0, \eta, \eta'$ ) at  $B^-$  factories: status and combinations*, *Nucl. Phys. Proc. Suppl.* **169** (2007) 199 [[hep-ex/0702017](#)] [[SPIRES](#)].
- [55] W. Rodejohann, *The see-saw mechanism: neutrino mixing, leptogenesis and lepton flavor violation*, *Pramana* **72** (2009) 217 [[arXiv:0804.3925](#)] [[SPIRES](#)].
- [56] F.R. Joaquim, *Predictions for  $L_j \rightarrow L_i$  gamma in the SUSY triplet seesaw mechanism: Large tan beta effects*, *Nucl. Phys. Proc. Suppl.* **188** (2009) 342 [[SPIRES](#)].
- [57] S. Davidson, *Parametrizations of the seesaw, or, can the seesaw be tested?*, [hep-ph/0409339](#) [[SPIRES](#)].
- [58] G.C. Branco et al., *Minimal scenarios for leptogenesis and CP-violation*, *Phys. Rev. D* **67** (2003) 073025 [[hep-ph/0211001](#)] [[SPIRES](#)].
- [59] C. Hagedorn and W. Rodejohann, *Minimal mass matrices for Dirac neutrinos*, *JHEP* **07** (2005) 034 [[hep-ph/0503143](#)] [[SPIRES](#)].
- [60] Y. Farzan and A.Y. Smirnov, *Leptonic CP-violation: zero, maximal or between the two extremes*, *JHEP* **01** (2007) 059 [[hep-ph/0610337](#)] [[SPIRES](#)].

- [61] DAYA-BAY collaboration, X. Guo et al., *A precision measurement of the neutrino mixing angle  $\theta_{13}$  using reactor antineutrinos at Daya Bay*, [hep-ex/0701029](#) [SPIRES].
- [62] DOUBLE CHOOZ collaboration, F. Ardellier et al., *Double CHOOZ: A search for the neutrino mixing angle  $\theta_{13}$* , [hep-ex/0606025](#) [SPIRES].
- [63] RENO collaboration, S.B. Kim, *RENO: Reactor experiment for neutrino oscillation at Yonggwang*, *AIP Conf. Proc.* **981** (2008) 205 [*J. Phys. Conf. Ser.* **120** (2008) 052025].
- [64] J. Hisano, T. Moroi, K. Tobe and M. Yamaguchi, *Lepton-Flavor Violation via Right-Handed Neutrino Yukawa Couplings in Supersymmetric Standard Model*, *Phys. Rev. D* **53** (1996) 2442 [[hep-ph/9510309](#)] [SPIRES].
- [65] PARTICLE DATA GROUP collaboration, C. Amsler et al., *Review of particle physics*, *Phys. Lett. B* **667** (2008) 1 [SPIRES].
- [66] A. Brignole and A. Rossi, *Anatomy and phenomenology of mu tau lepton flavour violation in the MSSM*, *Nucl. Phys. B* **701** (2004) 3 [[hep-ph/0404211](#)] [SPIRES].
- [67] SUPERKEKB PHYSICS WORKING GROUP collaboration, A.G. Akeroyd et al., *Physics at super B factory*, [hep-ex/0406071](#) [SPIRES].
- [68] M. Bona et al., *SuperB: A High-Luminosity Asymmetric  $e^+e^-$  Super Flavor Factory. Conceptual Design Report*, [arXiv:0709.0451](#) [SPIRES].